NASA Technical Memorandum 4523

ESTAR—The Electronically Scanned Thinned Array Radiometer for Remote Sensing Measurement of Soil Moisture and Ocean Salinity

C. T. Swift
National Aeronautics and Space Administration
Washington, D. C.

National Aeronautics and
Space Administration

Goddard Space Flight Center
Greenbelt, Maryland 20771

1993

FOREWORD

This report is the product of a working group assembled to help define the science objectives and measurement requirements of a spaceborne L-band microwave radiometer devoted to remote sensing of surface soil moisture and sea surface salinity. Remote sensing in this long-wavelength portion of the microwave spectrum requires large antennas in low-Earth orbit to achieve acceptable spatial resolution. The proposed radiometer, ESTAR, is unique in that it employs aperture synthesis to reduce the antenna area requirements for a space system.

Panel Members

Chairman:	C.T. Swift
Executive Secretary:	D.M. Le Vine
	J.A. Carton
	D.B. Chelton
	E.T. Engman
	A. Gordon
	T.J. Jackson
	G.S.E. Lagerloef
	E. Njoku
	I. Rodriques-Iturbe
	C.S. Ruf
	S. Sarooshian
	T.J. Schmugge
	R.A. Weller

I. EXECUTIVE SUMMARY

A. SOIL MOISTURE SCIENCE REQUIREMENTS

1. Introduction

The Earth's hydrologic cycle interacts with the land surface within a thin reservoir that stores and distributes precipitated water. This reservoir, commonly referred to as "soil moisture," plays a critical role in plant productivity, water storage, and both evaporation from the land and transpiration from plants. The water in the soil also alters its heat capacity and thermal conductivity, and buffers its temperature extremes. Model studies have consistently shown that surface soil moisture is an important boundary condition in long-range climate forecasting. Yet, despite its importance to the environment, very little quantitative information is available on the spatial and temporal patterns of soil moisture and their relationship to climate and hydrology. In fact, variations in soil moisture may be so great that point measurements—the conventional measurement tool—have little meaning. The practical result is that soil moisture is inadequately represented in current hydrologic, climatic, agricultural and biogeochemical models. This could change, however. Recent studies have demonstrated the ability of microwave remote sensing techniques to measure soil moisture, and a microwave sensor in space could provide the temporal and spatial sampling necessary for the inclusion of soil moisture in such models.

2. Instrument Requirements

Several surveys have identified the characteristics of an instrument capable of providing the soil moisture measurements that can elucidate the global hydrologic cycle (e.g., Rango *et al.*, 1980; Murphy, 1987). A summary of these requirements is presented in the table below:

MEASUREMENT REQUIREMENTS

Frequency	=	1.4 GHz
Polarization	=	Horizontal
Resolution	=	10 km
Sensitivity (ΔT)	=	1 K
Repeat Coverage	=	3 days

A frequency in the restricted band at 1.4 GHz offers penetration into the soil and minimizes the effects of vegetation canopy and surface roughness. At higher frequencies, both the attenuation due to vegetation and the decrease of the dielectric constant of water reduce the sensitivity of the measurement to soil moisture. Horizontal polarization is preferred because the Fresnel reflection coefficient varies slowly as a function of incidence angle (to about 40 degrees), making the measurement least sensitive to surface slope and look angle to the sensor. The spatial variability of soil moisture is driven primarily by variation in soil properties and the input flux, precipitation. The general consensus is that as far as the precipitation driven variations are concerned, a 10-km resolution with a repeat measurement every 3 days is adequate for most applications. Radiometric calibration to within a few degrees K will yield substantial information about surface soil moisture because the dynamic range of radiometric brightness temperature due to changes in soil moisture is very large (approximately 80 K). The scientific community's requirements depend on the application. The more demanding requirements range from a suggestion of 5 moisture levels (about 7 percent by volume; Rango *et al.*, 1980) to the 1-2 percent by volume desired by modelers hoping to use the surface measurement to retrieve moisture profiles or estimates of moisture in the root zone. Given that a change of 1-percent volumetric soil moisture corresponds to a change of 2-3 K, and that the accuracy of *in situ* point measurements of volumetric soil moisture is typically 3 percent (rms), a radiometric accuracy of 1 K is more than sufficient for even the more demanding use (Murphy *et al.*, 1987).

B. SALINITY SCIENCE REQUIREMENTS

1. Introduction

The salinity of water at the ocean surface is an important parameter in determining ocean circulation, air-sea coupling, and the influence of these processes on global climate. Ocean circulation is driven by the wind and by changes in surface water density in response to changes in temperature and salinity. The thermohaline component of circulation, while slower than the wind-driven surface currents, involves the full volume of the ocean and is capable of moving vast amounts of heat and water, as well as carbon in a variety of forms, between oceans. For example, in the northern Atlantic Ocean, warm and salty upper ocean water is cooled and sinks into the deep ocean, called the North Atlantic Deep Water (NADW). Ultimately, this water spreads across the South Atlantic and into the circum-Antarctic deep ocean belt, eventually reaching the Indian and Pacific Oceans. Ultimately the water returns to the surface and migrates back to the sinking regions to complete a thermohaline circulation cell in what is often referred to as a "conveyor belt." On the return leg of this conveyor belt, warm water is drawn toward the North Atlantic to compensate for the sinking NADW. If this process were to stop, estimates suggest that the northern Atlantic Ocean would be as much as 6 ° C cooler due to the decreased influx of warm water. This would induce a significant change in the climate of the Northern Hemisphere.

2. Instrument Requirements

The variation in salinity among the world's oceans is only a few parts per thousand (ppt), and it is estimated that in order for measurements of salinity in the open ocean to impact the under-

standing of ocean circulation and climate, an accuracy on the order of .05 ppt is desirable. Since these phenomena occur on a large scale and with a relatively long time constant, a spatial resolution of 100 km and an update of the global salinity map every 30 days is appropriate.

The requirements for a microwave radiometer system to conduct these measurements are listed in the table below.

MEASUREMENT REQUIREMENTS

Frequency	=	1.4 (2.65 & 5.0 GHz)
Polarization	=	Horizontal
Resolution	=	100 km
Sensitivity (ΔT)	=	.02 K
Repeat Coverage	=	30 days

Achieving a measurement accuracy of .02 K (which yields a salinity accuracy of .05 ppt; Klein and Swift, 1978) is a demanding requirement for a microwave radiometer in space, but it could possibly be met with conventional technology by trading spatial and temporal resolution for sensitivity. For example, given a radiometer with a sensitivity of 1 K, a spatial resolution of 10 km, and a revisit time of 3 days, and assuming independent pixels and pixel averaging in space and time, a measurement could be obtained every 100 km and 30 days with an effective sensitivity of about .02 K.

The thermal emission in the microwave region depends on both salinity and water temperature, and so two measurements are needed to obtain salinity. One possibility is to make measurements at 1.4 and 2.65 GHz (as demonstrated by Blume *et al.*, 1978), perhaps with an additional channel near 5.0 GHz to improve the temperature estimate. One could also use a single measurement at 1.4 GHz, where the sensitivity to salinity is strongest, plus an independent measurement of temperature, e.g., from climatological maps or the output from a sensor on another platform.

If the sensor is designed with a 10-km resolution, there may be applications in coastal regions, where accuracy as coarse as 2 ppt (corresponding to a radiometric sensitivity of 1 K) appears to be acceptable. Although 1-km spatial resolution is preferable for coastal zone mapping, with a resolution of 10 km one could produce coarse synoptic maps of entire continental shelves suitable for monitoring the mixing process as a function of tidal cycle, rate of precipitation, snow melthing, and so on.

C. APERTURE SYNTHESIS

This interferometric technique measures the complex correlation of the output voltage from pairs of antennas at many different baselines (Thompson, Moran, and Swenson, 1988). Each baseline produces a sample point in the two-dimensional Fourier transform of the scene. After all measurements have been made, a map of the scene is obtained by inverting the transform. Only one antenna pair is needed for each independent baseline, and small antennas can be used because the resolution is determined by how well the Fourier space has been sampled, not by the resolution of the actual antennas used in the measurement. A substantial reduction can thus be made in the antenna collecting area required in space.

Aperture synthesis could be implemented to make measurements from space in many ways (Le Vine *et al.*, 1989). Figure 1 shows an example based on a configuration already demonstrated in aircraft experiments that could achieve the requirements for the measurement of soil moisture and ocean salinity described above (Le Vine *et al.*, 1990, Swift *et al.*, 1991). This hybrid instrument uses real antennas to obtain resolution along track and employs aperture synthesis to achieve resolution across track. Aperture synthesis reduces the required antenna area by more than 80 percent, and the entire structure can be easily folded for packaging at launch.

OVERVIEW:

- THREE CHANNELS (1.41, 2.65, 5.00 GHz)
- 14 SLOTTED WAVEGUIDE ANTENNA ELEMENTS PER CHANNEL
- APERTURE SIZE = 44.8λ x 44.8λ AT ALL FREQUENCIES

ANTENNA ARRAY ELEMENTS:

FREQUENCY (GHz)	1.41	2.65	5.00
LENGTH (cm)	950.8	505.9	268.1
CROSS SECTION	STANDARD WAVEGUIDE		
WEIGHT (kg/ELEMENT)	6.6	1.5	0.5

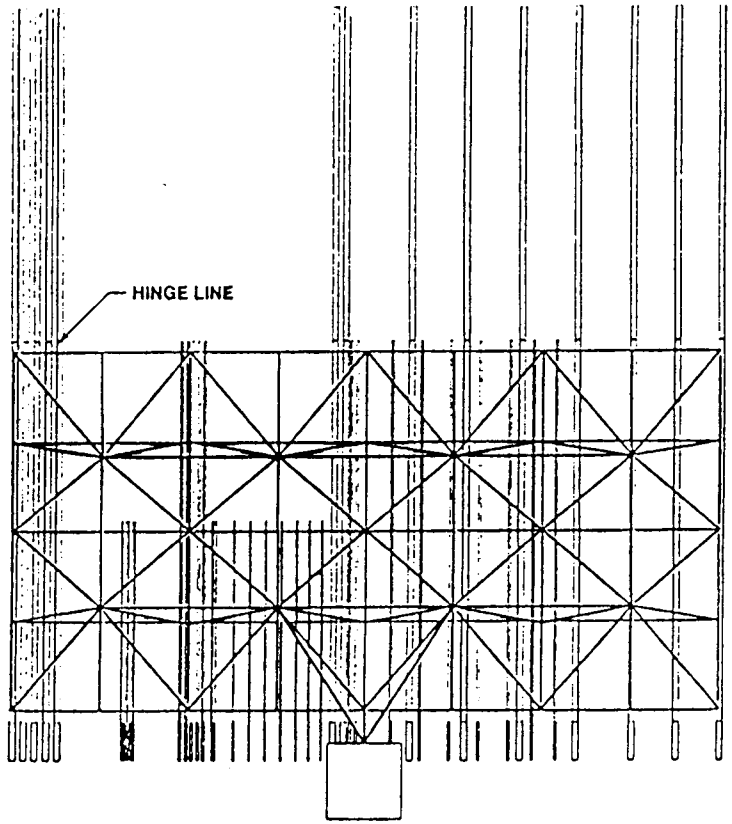

Figure 1. Three frequency synthetic aperture radiometer to make measurements of soil moisture and ocean salinity from space.

II. SURFACE SOIL MOISTURE

A. OVERVIEW

The Earth's hydrologic cycle interacts with the land within a thin reservoir that stores and distributes precipitated water. This reservoir, commonly referred to as "soil moisture," integrates much of the land surface hydrology and is the foundation for land-based life. As central as this is to human existence and to biogeochemical cycles, very little quantitative information exists on the spatial and temporal patterns of soil moisture and their relationships with climate and hydrology. A primary reason for this is the difficulty in measuring it, not at one point in time, but in a consistent and spatially comprehensive basis. Soil moisture exhibits such large spatial and temporal variability that point measurements have had very little meaning. Because of this lack of information, soil moisture has not been treated as a variable in hydrologic or land process models. However, the demonstrated ability of microwave remote sensing techniques for measuring soil moisture may change this.

Assuming a microwave remote sensing system in space, many applications could be made of the measured soil moisture. Among these are (Engman, 1992):

1. **Climate Studies:** Soil moisture is an indicator of changes in climate, an input for weather forecasting, and a boundary condition for General Circulation Models (GCMs).
2. **Water Budget Studies:** Soil moisture is a form of water storage; remote sensing can provide the needed temporal and spatial continuity to extrapolate water budget studies to larger areas.
3. **Precipitation Estimates:** Precipitation is the source of soil moisture and regular measurement of soil moisture could augment precipitation retrieval algorithms over land, where satellite measurement is most difficult.
4. **Agriculture:** A measurement of soil moisture would improve pest management techniques, crop yield models, and drought assessment.
5. **Flood Forecasting:** Soil moisture is an "initial condition" in the models on which forecasts are based, but very little information is currently available on this initial condition.
6. **Frozen Soils:** Identification of frozen soil has important applications in flood and runoff forecasts and in assessing crop damage assessments through winter kill.

The extent to which a passive microwave sensor in space can impact each of these applications will depend on the spatial and temporal resolution of the measurement. Some of the applications, notably those in process hydrology and small-scale agriculture, require spatial resolutions that are unlikely to be obtained with instruments available in the foreseeable future; however, other applications such as climate studies have spatial requirements well within the feasibility of current technology. Since this particular application could be easily addressed and is of such obvious importance to the continuing understanding of the environment, additional background on the role of soil moisture in global climate modelling is briefly described below.

B. SOIL MOISTURE IN GLOBAL CLIMATE MODELS

Water near the soil surface plays a fundamental role in climate through the redistribution of the energy associated with evapotranspiration. The importance of this emerged in the mid-1960s, when researchers at the Geophysical Fluid Dynamics Laboratory added a land hydrology component into their general circulation model (Manabe *et al.*, 1965; Manabe, 1969). More recently, a steady progression of research has shown the importance of surface moisture on the Earth's climate including the sensitivity of albedo to climate (Charney *et al.*, 1977) and the influence of soil moisture anomalies (Walker and Rowntree, 1977; Shukla and Mintz, 1982; Rowntree and Bolton, 1983).

This seminal research was conducted primarily by meteorologists and climatologists, without significant input from land-surface hydrologists, who were more concerned with the traditional problems of engineering hydrology focused on catchments. New interest in linking land surface hydrological processes to atmospheric processes has changed this emphasis, and hydrologists have begun to take an active role in large-scale field experiments. The objectives of these experiments are, first, the further understanding of land-atmospheric processes, with the aim of developing climate models with parameterizations that better represent processes (especially biophysical processes) and that account for spatial heterogeneity in these processes; and second, analysis of the effects of scaling well-represented, small-scale processes up to larger scales, including the scale of the measurement made by satellite remote sensing instruments. In both cases, the role of soil moisture is central because it plays a dominant role in controlling most land-surface processes.

1. Land Parameterizations and Climate Studies

Among climate modelers, the term 'parameterization' refers to the parametric representation of small-scale (or sub-grid scale) processes at large scales (or computational grid scale). Implicit in this definition is the concept that the small-scale processes have been scaled up in some appropriate fashion to adequately represent their influence at the large scale. This is in contrast with large-scale dynamics and thermodynamics of the atmosphere and oceans which are supposedly modeled to their precise physical laws.

During recent years, new parameterizations have attempted to overcome two major simplifications in the earlier parameterizations: 1) a simplistic soil moisture availability function based on field capacity and water budget accounting; and 2) evaporation modeling without explicit physiological resistance from vegetation. Modelling studies from the late 1970s and early

1980s show that precipitation and temperature are sensitive to soil moisture anomalies. One motivation to include the role of vegetation in the hydrologic cycle was the desire to study biosphere-climate interactions, since some of the most pressing questions include the large-scale climatic effects of deforestation and the loss of tropical rainforests.

Parameterizations that have fully developed biosphere-atmosphere interactions for calculating the transfer of energy, mass, and momentum between the atmosphere and the vegetated surface of the Earth have been developed by Dickinson *et al.* (1986), Sellers *et al.* (1986), and Abramopolous *et al.* (1988). Attempts to calibrate such detailed biosphere models have often relied on small-scale micrometeorological studies (Sellers and Dorman, 1987; Sellers *et al.*, 1989), but calibration data based on a small-scale field site could mask the performance of the land parameterization within GCMs because sub-grid variability may have significant effects. Recent work by Lakshmi and Wood (1991) has shown these parameterizations to be quite sensitive to soil moisture conditions. This supports field work on trace-gas fluxes from forest canopies in which the most significant factor controlling the spatial-temporal fluxes is soil moisture (Dlugi, 1991). Unfortunately, the detailed biospheric models are too complex to consider spatial variability in soil moisture due to variations in topography and soils. The impact on the model predictions is an area of active research, one that is being hampered by the lack of adequate sensors that can remotely measure soil moisture at adequate scales over large areas.

There is also interest in developing parameterizations simpler than those referenced above but nonetheless incorporating important features of the governing hydrological processes. In fact, these parameterizations try to include sub-grid variability associated with terrain, soil and vegetation inhomogeneities (Entekhabi and Eagleson, 1989; Avissar, 1990; Famiglietti and Wood, 1990; Wetzel and Chang, 1988). These analyses allow scientists to explore major model sensitivities to soil characteristics and climatic forcing. The effects from such heterogeneities can be significant, as shown by results in Avissar and Pielke (1989) and Avissar (1990). These simpler parameterizations must still be tested against more detailed parameterizations as well as verified against large-scale field data. Remotely sensed observations of soil moisture are needed to verify the hypothesized spatial variations in soil moisture, which are central to these model formulations.

2. Sensitivity Studies

Early studies with GCMs using land-surface parameterizations showed that strong feedback existed between soil moisture anomalies on the land and climate. These results have been repeated in more recent studies exploring these linkages. These studies are referred to here as sensitivity analyses since the research explores the sensitivity of climate to either atmospheric forcings or land-surface parameterizations.

Most sensitivity studies have focused on the influence of initially prescribed soil moisture levels on atmospheric variables such as precipitation and temperature. One such example is given by Oglesby and Erickson (1989), who describe a series of numerical experiments using NCAR's Community Climate Model. The experiments focused on the response of the atmosphere to soil moisture anomalies with particular reference to North American droughts.

Delworth and Manabe (1988, 1989) analyzed the influence of an interactive land hydrology on the temporal variability of computed soil wetness. As part of their study they also compared an interactive land-hydrology parameterization with a fixed (prescribed) surface wetness condition. Their results show that the interactive parameterization allows for larger variations in the energy fluxes, thereby increasing the variance of surface air temperature.

Most GCMs use spatially fixed land-surface parameterizations because of data availability problems. A critically important problem that must be resolved is the sensitivity of climate to spatial variations in these parameterizations—at both the GCM grid scale and as affected by sub-grid variability. Wilson *et al.* (1987) carried out sensitivity studies with different soil and vegetation parameters. The analysis was done with a standalone version of this land-surface scheme. They analyzed five different bioclimatic regimes: a low-latitude evergreen forest, a low-latitude sand desert, a high-latitude boreal forest, high-latitude tundra and a prairie grassland. The sensitivity experiments included changes in soil properties (including texture and the resulting hydraulic properties, depth, and albedo); as well as changes in vegetation characteristics such as stomatal resistance. The model results were most sensitive to variations in soil texture, particularly to the associated variations in hydraulic conductivity and diffusivity parameters that control infiltration and evaporation.

Soil hydraulic parameters significantly affect moisture transfers between the land and atmosphere. Wetzel and Chang (1986) examined the effect of natural soil variability on evapo-transpiration, and found that soil variability is large enough to seriously alter the relationship between regional estimates based on homogeneous grid-box assumptions and for spatially variable conditions. Avissar and Pielke (1989) carried out regional mesoscale studies using land surfaces with patch heterogeneity and found that such heterogeneities can affect latent and sensible heat fluxes by up to, and sometimes in excess of, 100%. Further, they also showed that these heterogeneities can generate circulations as strong as seabreezes. Sensitivity analyses in Entekhabi and Eagleson (1989) used sub-grid variability in soil wetness (modeled with a gamma probability function) to investigate sensitivities to soil type and climatic forcings on runoff, soil evaporation, and transpiration from vegetation.

3. Measurement Requirements

In reviewing the research to date, a key unresolved question is the level of detail required to specify the land hydrology, in terms of vertical resolution (vegetation and soil), horizontal heterogeneity, and temporal performance. To resolve this question will

require a two-pronged approach that includes interpretation of data from a range of local and regional-scale field experiments using the same atmospheric model and initial conditions. A spacecraft instrument used in conjunction with current and planned field experiments would provide this needed data.

A soil moisture measuring instrument in space with resolution on the order of 10-20 km would have sufficient resolution to help resolve these issues (e.g., using high-resolution data in conjunction with extensive field campaigns), and also would provide the boundary condition needed for global change models. Most models require input at 100-km resolution or greater. Hence, even at 20 km, adequate resolution exists to study effects of land-surface parameterizations.

C. PHYSICS OF MICROWAVE REMOTE SENSING OF SOIL MOISTURE

Microwave remote sensing, particularly at the long-wavelength end of the microwave spectrum, offers several advantages compared to other spectral regions. First, the atmosphere is almost transparent, minimizing atmospheric corrections and providing all-weather observations. Second, the measurements do not require solar illumination, which allows for day or night observation. Third, vegetation is semi-transparent at long wavelengths, allowing observation of the underlying surface. Finally, the dielectric constant of soil, and therefore its microwave brightness temperature is directly dependent on the amount of water present, providing a direct, physically interpretable measurement. (For example, at frequencies below about 5 GHz, the dielectric constant of water is approximately 80, whereas for dry soil it is between 3 and 4, depending on soil type. This large contrast provides the basis for estimating the moisture content.)

The microwave response to the soil-water mixture is determined by the product of the emissivity of the surface times its physical temperature. In the case of smooth surfaces, the emissivity is: $\varepsilon = 1 - |R|^2$ where R is the Fresnel reflection coefficient of the surface. The Fresnel reflection coefficient depends on the dielectric constant of the surface, and also the polarization and incidence angle of the observation. The emissivity varies from about .36 for wet soil to .99 for dry soil. Assuming a soil temperature of 290 K, this results in a change of brightness temperature from about 105 K for wet soil to 270 K for dry soil. This is a very large range compared to the 1-2 K typical of the accuracy achieved by radiometers employed in contemporary microwave remote sensing research.

D. SENSOR SYSTEM REQUIREMENTS

Among the most important system design parameters is the selection of the wavelength. One reason for this is that the contrast in dielectric constant of water and dry soil is frequency-dependent and the contrast decreases as the frequency increases above about 5 GHz. A second reason is that the sensitivity to surface soil moisture is decreased by the presence of a vegetation canopy. For the same canopy and vegetation water content, the sensitivity is reduced as the frequency increases. The sensitivity over bare soil remains about the same up to a frequency of 5 GHz, but when vegetation is present, the loss of sensitivity at this frequency is significantly reduced (Jackson *et al.*, 1982; Wang, 1985). In general, longer wavelengths are more desirable for soil moisture estimation.

Typical relationships between soil moisture and microwave brightness temperature are shown in Figure II.1. Figure II.1a shows the relationship at L-band as a function of vegetation water content. The slope of each curve is a measure of the sensitivity of the measurement, and in Figure II.1b these sensitivities are plotted as a function of frequency for various values of vegetation water content. The results shown in Figure II.1b are computed results using a microwave simulation model.

A final consideration in frequency selection is the depth of the soil layer that contributes to the measured brightness temperature. Radiative transfer theory shows that the brightness temperature observed by a sensor is the integrated result of the dielectric properties in a layer and that the effective depth of this layer (5 - 10 cm at L-band) increases with wavelength. Obviously, a deeper sensing depth is desirable because it provides the most information on the soil profile. In addition, the depth that is sensed will impact on the revisit time required of the observations. For precipitation studies, the "memory" of the surface soil becomes shorter as the wavelength (and therefore depth sensed) decreases. Longer wavelengths allow more flexibility in frequency of coverage.

In addition to wavelength, polarization and look angle must be considered. Figure II.2, where the sensitivity of the measurement is shown as a function of look angle at L band, illustrates the effects of polarization. Horizontal polarization is preferred because the sensitivity to moisture is higher at all look angles for both bare and vegetated fields.

The ability to use as wide a range of look angles as possible is desirable in any mapping system, and the effects of look angle can be compensated for in the data interpretation algorithms. There are two competing factors at work that must be considered: the change in sensitivity with look angle and the increase in the path length through the vegetation. As Figure II.2 indicates, these two factors tend to offset each other for horizontal polarization. Based upon these considerations, the choice of look angle for horizontal polarization is not critical. The negative aspect of larger look angles is that the size of the footprint increases with look angle.

E. REMOTE SENSING HERITAGE

As part of research to develop remote sensing techniques for the measurement of soil moisture from space, there has been an ongoing program of aircraft experimentation and a short-lived Skylab experiment with an L-band radiometer.

The majority of the aircraft data available for analysis comes primarily from two L-band systems: a single beam system that was flown on NASA P-3 and C-130 aircraft from the mid 1970s until the early 1980s (e.g., Jackson *et al.*, 1989), and a pushbroom microwave radiometer (PBMR) configured for 3 or 4 beam positions that has been flown on a NASA Skyvan, P-3, and C-130 aircraft since 1983 (Harrington and Lawrence, 1985; Schmugge *et al.*, 1992). In addition to these sensors, there is a great deal of aircraft L-band data collected by scientists in the former USSR and summarized in Shutko (1986). Currently, several systems are flying operationally in the former USSR, Hungary and Bulgaria. An Italian research group (Pampaloni *et al.*, 1990) has recently integrated an L-band sensor into their research aircraft package. A French research group (CNES) is also developing an aircraft radiometer package.

The essential relationship between emissivity and surface soil moisture was verified early in the aircraft studies. An example of these results is those reported by Jackson *et al.* (1984) for a multiyear experiment over rangeland watershed sites in Oklahoma. Figure II.3a shows the L-band observations and Figure II.3b is a plot of the C-band observations. The data were collected simultaneously near nadir at horizontal polarization. These graphs illustrate the loss in sensitivity in going from L to C band. The total range in observed emissivities has been nearly cut in half.

Figure II.3a also includes data collected during 1980 at 10 times the baseline altitude, which increased the sensor footprint size from 75 to 750 m. The high-altitude observations appear to follow the same trend as the lower altitude data. Also plotted in Figure II.3a are data collected over similar sites in the Konza Prairie in 1985 as reported by Schmugge *et al.* (1988). These data were collected with the PBMR and show consistency between the two radiometer systems in different areas.

The PBMR program for soil moisture was initiated because the ability to collect brightness temperature maps within a reasonable time opened new opportunities to study the spatial and temporal dynamics of surface soil moisture or emissivity. This is also one of the reasons for developing a spaceborne sensor.

The first large-scale application of the PBMR was in the HAPEX experiment conducted in France in 1986. Due to a limited range of observed conditions, these data have not been extensively processed. In constrast, data from the second project to use the PBMR, the 1987 FIFE program, has been extensively analyzed. As part of this project, an area 7 by 14 km was mapped a total of 11 times. The resulting brightness temperature maps clearly reflected the antecedent meteorological conditions (Wang *et al.*, 1990). Comparisons with ground observations of surface soil moisture showed that moisture could be determined from the radiometer data after some calibration, and soil moisture maps have been developed for selected watershed sites.

The FIFE results have stimulated many researchers interested in the spatial and temporal dynamics of the surface soil moisture. As a result, the PBMR instrument was involved in two major hydrologic/meteorological experiments during the summer of 1990, MONSOON '90 and MACHYDRO '90. MONSOON '90 was conducted on the Walnut Gulch watershed, an arid rangeland site in southeast Arizona. Over a 10-day period, a total of six PBMR mapping missions were conducted (Schmugge *et al.*, 1992).

In August of 1991, the prototype ESTAR instrument was flown on the C-130 over the Walnut Gulch watershed. Meteorological conditions during the experimental period resulted in ground moisture values that produced the full range of brightness temperatures observed during MONSOON'90. Two days prior to the first flight conducted on August 1, there was a localized rainfall event centered in the southeast. An isohyetal map for the rainfall during this event was produced using data collected by 84 rain gages distributed over the area and the result is shown in Figure II.4a. On the day before the second flight on August 3, a large cellular rainfall event occurred centered in the northeast. Figure II.4b shows the isohyetal map for this event. The resulting brightness temperature maps for the two dates are shown in Figures II.5a and II.5b.

The brightness temperature patterns of Figure II.5 match the rainfall patterns presented in Figure II.4 for the respective dates. Further analysis of the data (Jackson *et al.*, 1993) has shown that the ESTAR data can be used to quantitatively estimate the spatial distribution of rainfall. These results indicate that the brightness temperatures yield the same basic results as those obtained using the rain gages. This suggests a potential way to greatly enhance our ability to estimate rainfall over large and remote areas that typically do not have rain gage networks. Using a limited rain gage network, a basic functional relationship could be established, and then used with the microwave brightness temperature. If the characteristics of this function can be related to local features, the results could be extrapolated over very large regions.

The data available from satellite platforms are quite limited. All the spaceborne microwave radiometer systems that have flown to date have had either poor resolution (Skylab L band) or short wavelengths (Nimbus ESMR, SMMR and SSM/I). Even with these drawbacks however, investigators have been able to verify the basic ability of these instruments to measure soil moisture from a satellite platform. Another problem with these investigations has been that little (if any) actual ground observations of soil moisture were collected. As a result, investigators have used a soil moisture surrogate variable called the antecedent precipitation index (API), which incorporates the antecedent precipitation with a drydown correction typical of the season and region. Skylab had a nonscanning 21-cm radiometer with a 100-km field of view. McFarland (1976), Eagleman and Lin (1976), and Wang (1985) have used this radiometer to determine and map the API. These authors report correlations between the satellite and meteorological estimates of API to be between 0.85 and 0.96 in Texas and Oklahoma.

A number of other investigations have shown that shorter wavelength satellite systems could be used to estimate moisture-related variables (Schmugge *et al.*, 1977; Blanchard *et al.*, 1981; Choudhury and Golus, 1988; and Kerr and Njoku, 1990). These investigations have shown encouraging results; however, they

must be interpreted with some caution because they usually deal with a very limited geographical regions and typically only those with light vegetation covers. Under such conditions it is not unusual for the shorter wavelength systems to provide some useful information.

An example of this is a recent study by Heymsfield and Fulton (1992) using short-wavelength passive microwave radiometers for extracting rainfall information. The data from the SSM/I satellite (19, 37, and 86 GHz) were obtained for Oklahoma and Kansas following very large rainfall events that in some areas produced 15 cm of rainfall. Brightness temperature patterns from data collected during the event indicated that the 86-GHz data were correlated to ongoing rainfall whereas the 19-GHz data appeared to be dependent on the antecedent rainfall.

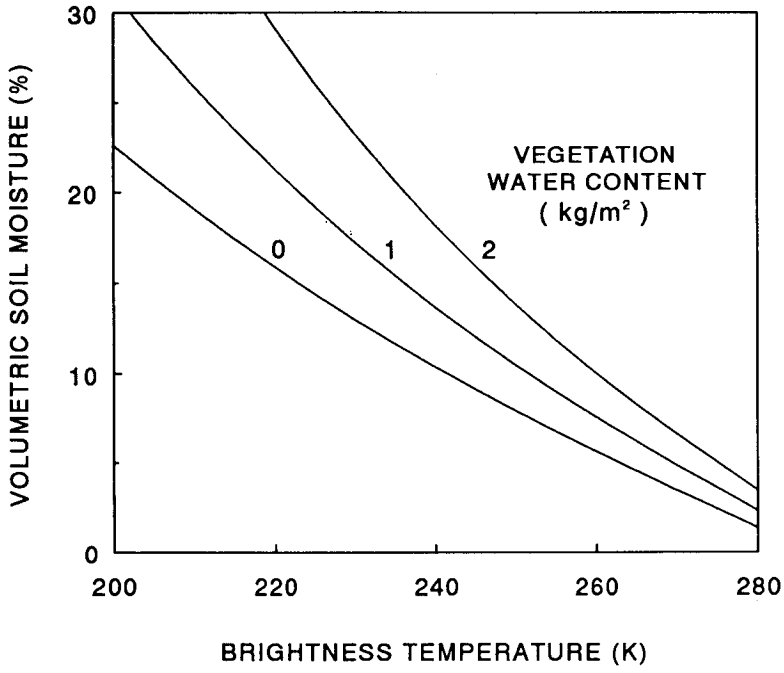

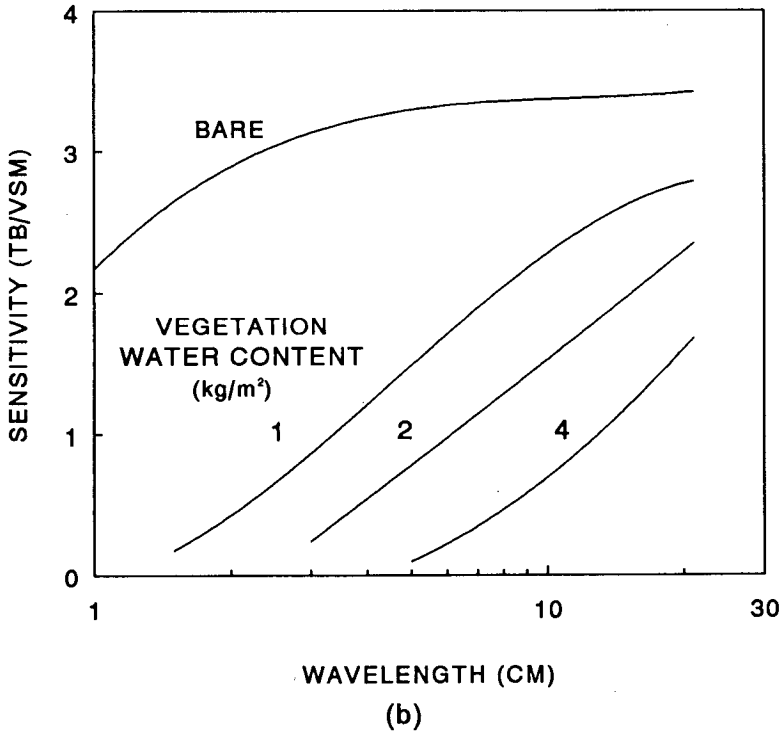

Figure II.1. a) The relationship between brightness temperature and volumetric soil moisture at L-band (H polarization 10° look angle) and b) sensitivity of brightness temperature to soil moisture as a function of wavelength for bare and vegetated conditions (H polarization 10° look angle).

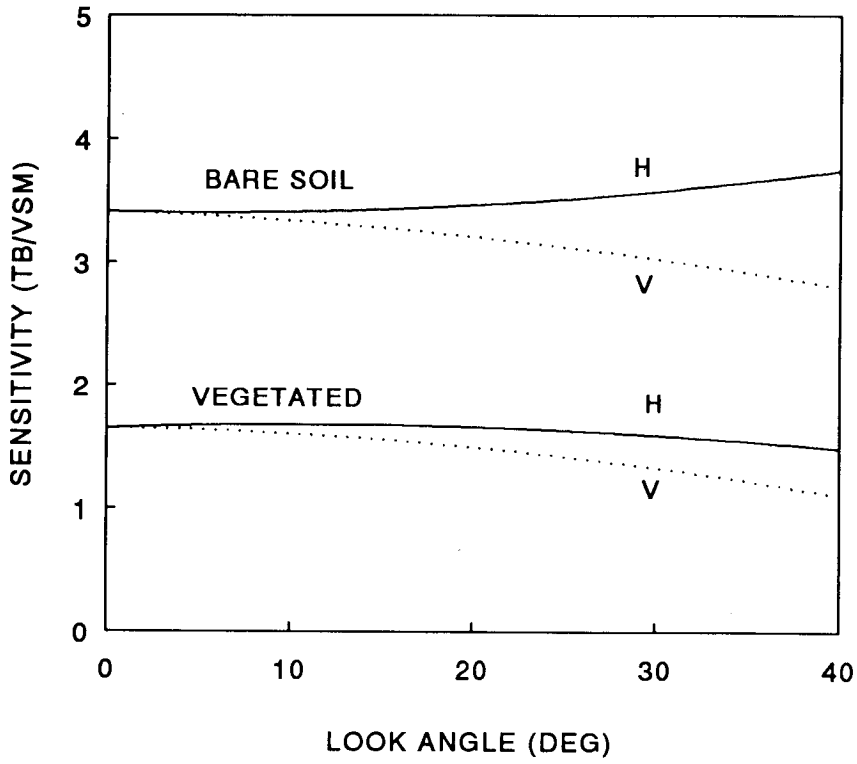

Figure II.2. Sensitivity of brightness temperature to soil moisture as a function of look angle for H and V polarizations (L band).

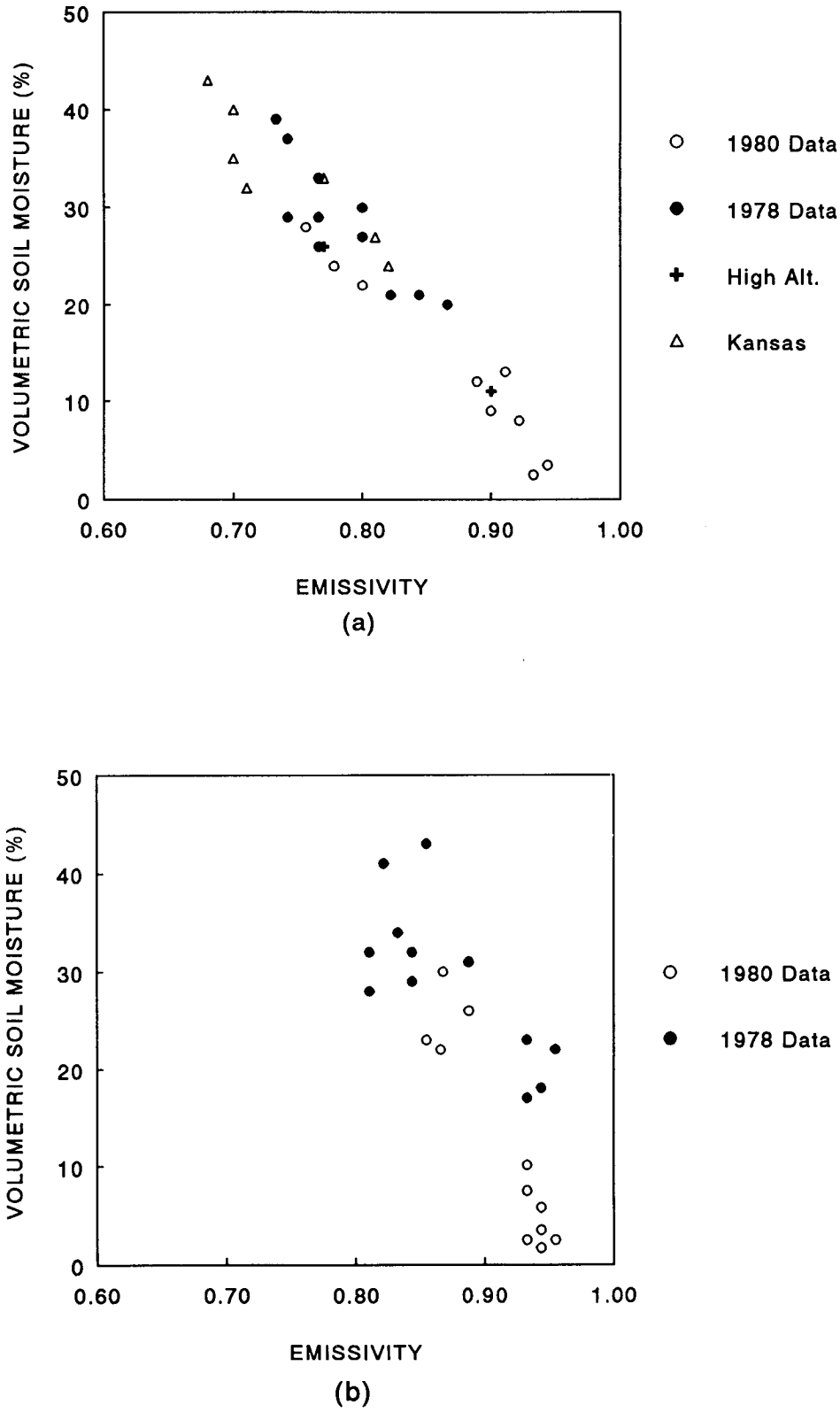

Figure II.3. Aircraft observations of emissivity and volumetric soil moisture (0-5 cm) for rangeland sites from Jackson *et al.* (1984): a) L-band data and b) C-band data.

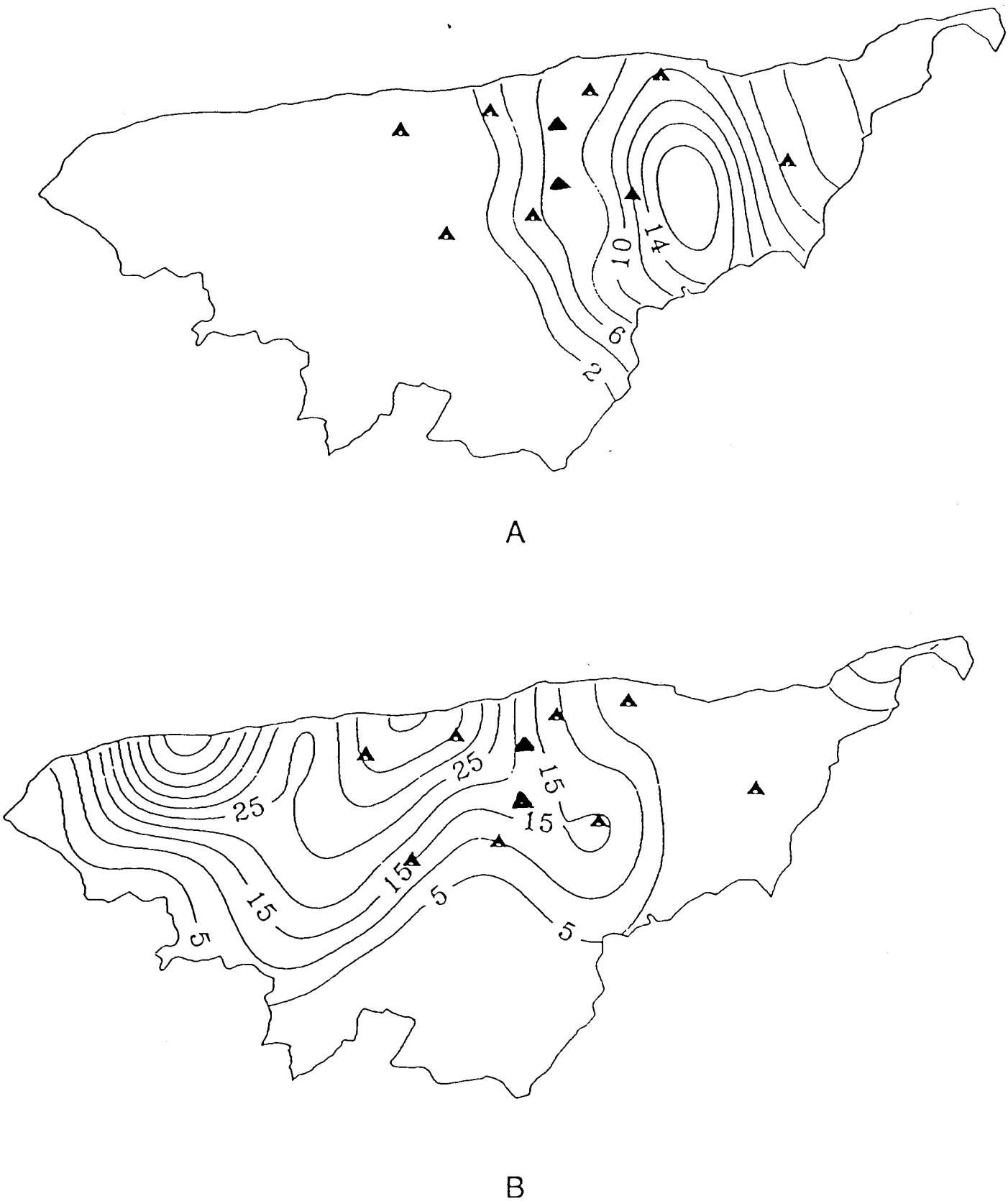

Figure II.4. Walnut Gulch rainfall maps derived from precipitation gage network; a) day July 30 and b) August 2.

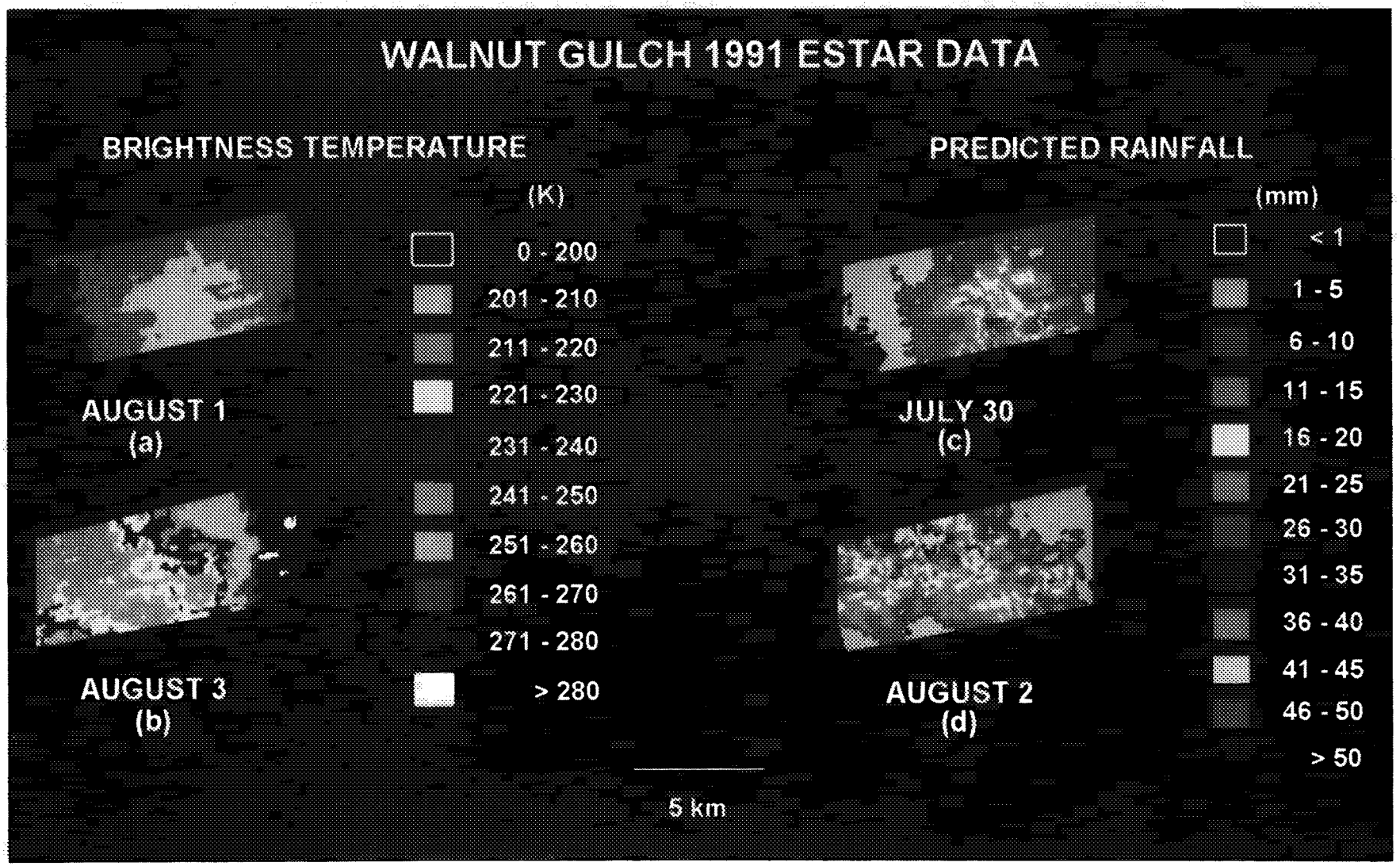

Figure II.5. Walnut Gulch 1991 ESTAR brightness temperature maps on a) August 1, and b) August 3; and predicted antecedent rainfall on c) July 30, and d) August 2.

III. REMOTE SENSING OF OCEAN SURFACE SALINITY

A. OVERVIEW

Remote sensing instruments can observe the oceans, measuring sea surface temperature, surface topography, surface winds, ocean color and other derived variables. Space-based remote sensing of surface salinity—an ocean parameter of considerable dynamical importance—has however, lagged in development, even though its principles have been understood for almost two decades. However, recent advances indicate that this could change. Chief of these is an increased awareness of the critical importance of surface salinity to deep convection of the oceans and tropical air-sea coupling, and the influence these processes have on global climate. In addition, recent microwave sensor technology which makes high spatial resolution from space feasible at long wavelengths, suggests that one should be able to observe salinity with a precision that approaches scientifically useful criteria.

This review addresses the present status of remote sensing of salinity, first discussing the scientific merits, then, assessing the potential performance of a modern sensor concept and the scientific questions that can be studied with data from such a system.

B. THE ROLE OF SALINITY IN OCEAN CIRCULATION AND THE GLOBAL CLIMATE SYSTEM

The ocean has a considerable influence on climate from geological timescales to the interannual variations such as the El Niño - Southern Oscillation (ENSO). It is hypothesized, for example, that the ocean moderates the warming rate induced by the greenhouse effect. It does this in two ways: absorbing excess greenhouse gases (carbon dioxide, methane and chlorofluorocarbons) from the atmosphere, and by absorbing some of the greenhouse-induced heat. The global average atmosphere temperature might be 1 to 2 ° C warmer were it not for the effects of the ocean. Considerable evidence also suggests that major changes in the oceanic circulation are linked to major climate shifts during and between ice ages. To understand these mechanisms, oceanographers must resolve, among other things, the general ocean circulation and its variability. This, in turn, requires a better understanding of the distribution and variability of surface salinity. Low surface salinity caps the ocean, attenuating convection and deep-reaching water-mass formation. With the proper amount of surface cooling at high latitudes, high surface salinity allows deep convection and ventilation of the interior of the ocean.

Clearly, a far better assessment of the hydrological budgets that control surface salinity must be developed, and we must be able to globaly monitor surface salinity. This is important for understanding both long-term climate change and the interannual variations in climate and weather.

To put this in context, it is necessary to understand how ocean circulation regulates climate, and the role that surface salinity plays in the ocean circulation processes. The ocean consists of nearly 1.4 billion cubic kilometers of salty water, about 97 percent of all water on the Earth. This enormous body of water exerts a powerful influence on Earth's climate by transporting heat, water, and other climate-relevant properties across great expanses of ocean, and by exchanging these properties with the atmosphere. Ocean circulation is driven by wind and the exchange of heat and water between the ocean and the atmosphere. In the tropics—particularly the Pacific—these air-sea fluxes and the dynamics peculiar to the equatorial circulation govern the 4- to 6-year ENSO cycle, which has far-reaching impacts on global weather. In contrast, the thermohaline circulation is much slower, involves the full volume of the ocean, and is capable of moving vast amounts of heat, water, and a variety of forms of carbon between oceans, thus modulating climate on much longer timescales. To gain a predictive capability about our changing climate we must understand the role of salinity in the thermohaline circulation and the tropical ocean/atmospheric dynamics.

1. Thermohaline Circulation and Long-Term Climate Change

In the northern North Atlantic and around the Antarctic, dense surface water sinks into the deep ocean to initiate the deep convective thermohaline circulation. Unique combinations of temperature and salinity are required to initiate sinking. If the surface salinity is too low, the water would not be dense enough to sink into the deep ocean, even if it were at the freezing point. In the Southern Hemisphere, upwelling of deep water, long removed from direct contact with the atmosphere, is quickly converted to cold, denser water to reenter the deep and bottom layers of the ocean. In the North Atlantic, however, thermocline water with a long history of contact with the atmosphere is cooled and sinks as relatively salty water into the deep ocean. The long contact these waters have with the atmosphere prior to sinking makes them well suited to satellite monitoring. The sunken water masses spread throughout the ocean and force the resident deep ocean water, which has been made more buoyant by downward diffusion of heat, to slowly rise. Eventually the upwelled water migrates back to the sinking regions to complete a thermohaline circulation cell or what is often referred to as a "conveyor belt," as indicated in Figure III.1 (from Broecker, 1991).

The North Atlantic is a relatively salty ocean: approximately 1.4 ppt higher at the depth of the thermocline than the North Pacific, for example. This high salinity sets the stage for deep convection, since with moderate cooling, the surface water becomes sufficiently dense to sink to the deep and bottom ocean, forming a deep water mass called North Atlantic Deep Water (NADW). As surface water sinks to produce NADW, it is transported at depth to the South Atlantic and other oceans, and

a compensating amount of thermocline and intermediate water masses from the world ocean is drawn towards the North Atlantic, where excess evaporation increases its salinity. The resultant thermohaline circulation cell strongly influences the Atlantic's poleward heat and salt fluxes. If NADW formation were to cease, estimates suggest that the surface water of the northern North Atlantic would be up to 6 ° C cooler, as the compensating flow of warm water into the North Atlantic would diminish. The presence of the warm water drawn into this region by NADW formation supports large heat losses to the atmosphere, mainly by enhancing evaporation from the ocean, moderating the climates of northern Europe.

The link between the supply of the warm salty surface water and continued sinking makes the NADW formation a constant process. Nevertheless, there is convincing evidence that surface salinity fluctuations in the high-latitude North Atlantic modulate the thermohaline circulation by altering NADW formation (Lazier, 1988; Dickson *et al.*, 1988). One possible mechanism is the capping of the surface ocean with less dense, low-salinity water from the Arctic Ocean. During the last century, at least two episodes of low surface salinity water occurred in the northern North Atlantic, drastically reducing or halting convection and NADW production. The most recent of these happened during the late 1960s and 1970s, and is referred to as the Great Salinity Anomaly, (Dickson *et al.*, 1988). Walsh and Chapman (1990) believe that these features originated with low-salinity outbreaks from the Arctic through Fram Strait and were also associated with anomalously expanded sea-ice cover in the regions of Iceland and the Labrador Sea. These large pools of lower salinity migrated about the northern North Atlantic, tracking the sub-polar gyre, and reduced NADW formation rates en route. The NADW recipe may be quite variable as the production rate of each component changes, over a variety of timescales, and for a variety of reasons. Many questions can be asked about these pools of low surface salinity: What are their spatial and temporal characteristics? Where do they come from? How large a freshwater anomaly is required to shut down NADW formation? The larger scale climatic importance of anomalous surface salinity pools in governing the depth of convection and NADW formation rates in the northern Atlantic makes the measurement of surface salinity a priority for monitoring the ocean.

The stability of the formation rates of the varied forms of NADW is one of the major concerns in evaluating future climate change. Changes in the 20th century related to the Great Salinity Anomaly are small compared to the suspected changes in NADW formation rates during the swings between glacial to interglacial periods. During the disintegration of the ice sheets from the last glacial epoch, a series of sudden injections of meltwater into the North Atlantic induced low salinity surface water and dramatic reduction of NADW formation. The strongest such event occurred 10,500 years ago when glacial meltwater was diverted from the Mississippi River to the St. Lawrence drainage system. The Younger Dryas cooling, a sudden re-advance of glaciers and a global-scale climatic cooling has been attributed to this event (Broecker and Kennett, 1989). This suggests that the ocean can change from a condition comparable to the modern, vigorous NADW formation state to a low NADW production state characteristic of the last glacial maximum in 300 years or less.

2. Tropical Ocean Atmosphere Interactions and Interannual Climate Variability

The Tropical Ocean Global Atmosphere (TOGA) research program has increased understanding of surface heat fluxes, the wind-forced redistribution of upper ocean heat in the tropics, and the feedback to the atmospheric circulation systems. However, surface freshwater flux and surface salinity on the upper ocean dynamics of the tropics has received far less attention. Buoyancy flux from excess precipitation in the South Pacific Convergence Zone (SPCZ) and Intertropical Convergence Zone (ITCZ) may contribute significantly to the buildup of upper layer volume in the western Pacific preceding and during ENSO events, and thus may be a fundamental process in the ENSO cycle.

The western equatorial Pacific is characterized by high sea surface temperature (SST), often referred to as the "warm pool," and by light winds and heavy precipitation as shown in Figure III.2. Present estimates of the annual mean net freshwater flux (precipitation-evaporation) in the warm pool are about 1.5 meters/year. This flux lowers surface salinity and stabilizes the surface water, making it very sensitive to changes in the air-sea fluxes of heat and momentum. Salinity effects complicate the air-sea interaction in the warm pool region, and there appear to be important feedbacks between SST, precipitation, upper ocean salinity, and wind-induced mixing. The inclusion of these feedbacks in coupled ocean-atmosphere models of the tropical Pacific are necessary for improved simulation of certain important features of ENSO and its effects on the global atmosphere. Interannual variations of surface salinity in the warm pool region are associated with changes in winds and rain that occur as part of the ENSO phenomenon; these variations may actively influence the development of ENSO.

The tropical Atlantic, in contrast, is a zone of net water loss by evaporation to the atmosphere, with more water flowing in from the south than leaving the north. The contribution of river discharge is much smaller than either evaporation or rainfall, except in the vicinity of the Amazon outflow. Rainfall is concentrated in the region of the intertropical convergence zone (ITCZ), but it does exceed evaporation by 15 cm/month, while in the subsidence zones of the northern and southern subtropics, evaporation may exceed rainfall by as much as 10 cm/month (Yoo and Carton, 1990). As the ITCZ shifts poleward following the seasonal shift of the sun, it creates strong seasonal fluctuations in rainfall and river discharge. These seasonal shifts, modulated by a complex interplay with seasonal changes in the advection patterns of the tropical currents, are reflected in changing patterns of sea-surface salinity. The strongest such annual changes occur in the western tropical region as indicated in Figure III.3.

C. MEASURING SURFACE SALINITY FROM SATELLITES: SENSOR REQUIREMENT

The above discussions illustrate the scientific importance of surface salinity to the general ocean circulation, air-sea interaction, and climate variability. Nevertheless, the straightforward observation of salinity remains a major challenge. *In situ* surface salinity measurements require more effort and specialized equipment than the measurement of temperature, consequently salinity measurements are considerably scarcer. Figure III.4 shows the surface salinity field, as presently known, based on the Levitus Atlas (Levitus, 1982). It is important to recognize that these data are, in reality, very sparse. The quality of this estimated field varies considerably by locale. If the global ocean were to be divided into boxes of 1 degree latitude by 1 degree longitude, only about 53 percent of those boxes would contain data. The average number of samples in the boxes that do contain data is only 18, and they are concentrated in the Northern Hemisphere regions of the ocean, which traditionally have been studied. Such a sparse data set makes it impossible to establish a reliable climatology of the global surface-salinity field, and to make any meaningful progress in understanding the links between salinity variations and the ocean circulation and climate variations.

A satellite system with a 10-km resolution and a 3-day revisit time would yield about 1000 observations per 1-degree box per month. Such a wealth of data clearly has the potential to provide far more information about the global salinity field and its variability than any conceivable *in situ* observing system. Preliminary estimates (e.g. Blume *et al.*, 1978; Swift and McIntosh, 1983) suggest that an accuracy of 1 ppt is reasonable from space. Assuming that a measurement with this accuracy can be obtained with 10-km spatial resolution and a sample interval of 3 days (e.g., using the L-band instrument proposed for EOS; Murphy *et al.*, 1987; Le Vine *et al.*, 1989), it is conceivable that by averaging over 100-km squares and up to monthly time intervals, the rms noise level of the sensor could be reduced to the neighborhood of 0.05 ppt. This would be adequate to resolve many of the oceanographic signals of significance discussed below. Of course, this assumes independent and unbiased samples, which may be difficult to obtain over long timescales. To do so would require extensive *in situ* salinity observations to provide precise calibration for the satellite system, and would also be warranted for such critical ocean regimes as the northern North Atlantic and tropical Pacific. The primary advantage of *in situ* salinity measurements is their accuracy, although the data are scarce. The primary advantage of data obtained through satellite remote sensing is the density of samples, but at a cost in accuracy.

Figure III.5 illustrates the potential usefulness of high-accuracy satellite measurements. The figure shows frequency spectra for two long (>25 years) surface salinity time series from the North Pacific at Station Papa and Hawaii (courtesy of S. Tabata and G. Broelert, respectively). Also shown are the equivalent noise levels for satellite salinity data (assuming a basic measurement with 10-km resolution, a revisit time of 3 days and rms noise equivalent to 1.5 ppt) after averaging over 10, 50, 100 and 500 km. These show that for the 100-km averages, the seasonal and interannual timescales are resolved significantly above the noise. Figure III.6 shows a similar exercise in the wavenumber domain based on a salinity transect between Alaska and Hawaii (courtesy of T. Royer). This time, the noise levels for different periods of temporal averaging are shown and suggest that the mean annual surface salinity can be resolved for spatial scales on the order of 100 km and larger. From these two spectral graphs, it is possible to illustrate the trade-off between spatial and temporal averaging with a simple curve showing the boundary between noise- and signal-dominated data as a function of space and timescales (Figure III.7).

It is pertinent to speculate whether a high-precision satellite sensor could have detected the "Great Salinity Anomaly" in the sub-Arctic Atlantic discussed above (Dickson *et al.*, 1988). Since the sensitivity to salinity decreases with temperature (e.g., Figure III.9), assume the achievable accuracy is reduced by a factor of two to 0.1 ppt (i.e., with averaging over 100 km and 1 month). The surface anomalies described by Dickson *et al.*, (1988) ranged from 0.1 to greater than 1.0 ppt on interannual timescales. This is significantly above the anticipated noise suggesting that, had it been in operation at that time, a satellite sensor would have been able to trace the "Great Salinity Anomaly."

Another view of how well a sensor in space might measure salinity variations is illustrated with an extensive tropical Pacific surface salinity data set accumulated by the French ORSTOM SURTROPAC group in New Caledonia (Delcroix and Masia, 1989). Figure III.8a is a surface contour plot of surface salinity along a near-meridional transect at about 160° E, between 28° S and 28° N, from 1969-1988. The data are composited monthly values every 2 degrees of latitude. A satellite sensor sampling this field as described above would make about 4000 observations in a 2x2 degree box every month, which, if averaged, would yield a residual sensor noise of about .02 ppt for monthly values. Addition of such noise to the data, Figure III.8b, illustrates that the interannual surface salinity variability in this SURTROPAC data is not obscured by this noise level, and should be resolved with a satellite sensor of the precision described here.

D. MEASUREMENT PHYSICS

The emissivity of sea water is a function of both salinity and temperature (e.g., Klein and Swift, 1977; Swift, 1980), and as a result, two measurements are necessary to retrieve salinity. These could be measurements at two microwave frequencies or a measurement of microwave brightness temperature and plus an independent measurement of water temperature. The relationship between microwave brightness temperature and salinity and water temperature is shown in Figure III.9 (from Swift and McIntosh, 1983) at L band. The relationship is a function of frequency and the sensitivity to salinity decreases as the frequency increases. Since L band is the lowest practical frequency for making measurements from space, it is also the optimum frequency for monitoring surface salinity. Also, notice that the sensitivity of

the measurement to salinity decreases with a decrease in temperature, although the relationship is relatively insensitive to temperature in the range of temperatures normally encountered in the oceans at mid-latitudes. Finally, the dependence of the relationship on polarization and incidence angle is governed largely by the Fresnel reflection coefficient of the surface although one would expect some small effects due to surface roughness.

E. HERITAGE

Several experiments have retrieved salinity from airborne microwave radiometers. Thomann (1976) reported measurements using an L-band radiometer (1.4 GHz) and an infrared radiometer (to provide the required surface temperature). Measurements were made in conjunction with surface truth in the vicinity of the Mississippi River, and good agreement was obtained for salinity concentrations ranging from 5 to 30 ppt. Measurements have also been made using two microwave frequencies at 1.4 and 2.65 GHz (Blume *et al.*, 1978; Blume and Kendall, 1982). Flights made over a series of parallel east-west flight lines obtained data for synoptic maps of the salinity field in the vicinity of the mouth of the Cheasapeake Bay. Comparison with surface measurements indicated an agreement of better than 1 ppt. Recent measurements were made using the ESTAR airborne L-band radiometer to detect salinity changes in the open ocean, where the range of salinity values is small (33-37 ppt) compared to those encountered in coastal and estuarian settings. In this experiment a flight was made from the coast (near the Maryland-Virginia border) to the center of the Gulf Stream. Preliminary data clearly show a trend in salinity values from the 32 ppt typical of coastal waters to the 36 ppt characteristic of the Gulf Stream (Lagerloef *et al.*, 1992).

The feasibility of measuring salinity from space using the L-band radiometer which was aboard Skylab in 1973 (Lerner and Hollinger, 1977) has also been tested. Figure III.10 (Lerner and Hollinger, 1977) shows that after correcting for other effects, the microwave brightness temperature shows a significant dependence on salinity. The surface salinity data were obtained from general ocean climate atlases rather than simultaneous surface observations, and the radiometer did not have the precision of a system designed to measure salinity. Nevertheless, the experiment demonstrates that it is possible to measure salinity from space.

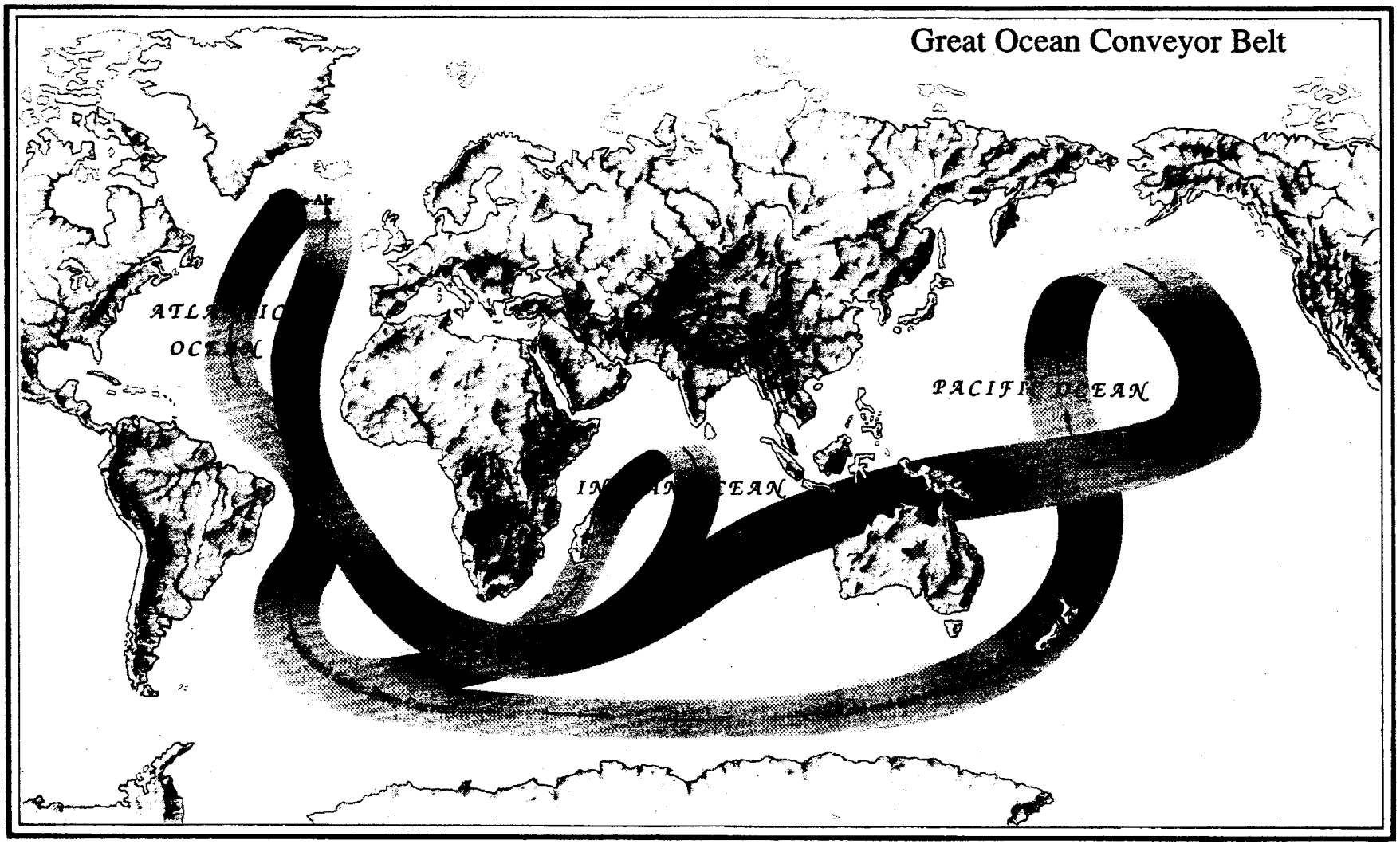

Figure III.1: The Great Ocean Conveyor (Broecker, 1991; illustration by J. Le Monnier), depicting the large-scale thermohaline ocean circulation which ventilates the deep ocean and has a regulating effect on climate over long timescales. Evidence suggests that, in the past, significant reductions of surface salinity in the far North Atlantic have interrupted or slowed the dense water formation and sinking, shutting down the convection and restricting the northward surface transport of warm water, with consequential climate cooling in the Northern Hemisphere.

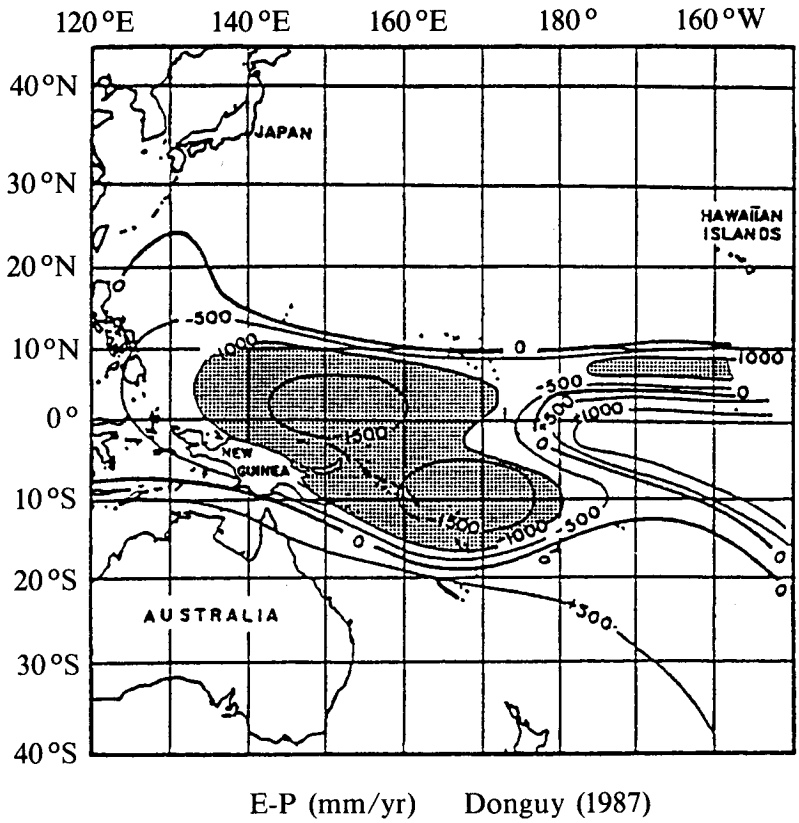

Figure III.2: The annual mean net evaporation minus precipitation (E-P) in millimeters (Donguy, 1987). Negative values indicate that precipitation exceeds evaporation. The regions of net surface freshwater flux into the ocean of more than one meter per year are shaded. The buoyancy accumulation associated with this freshwater flux affects the upper ocean dynamics, air-sea energy fluxes and the interannual El Niño-Southern Oscillation.

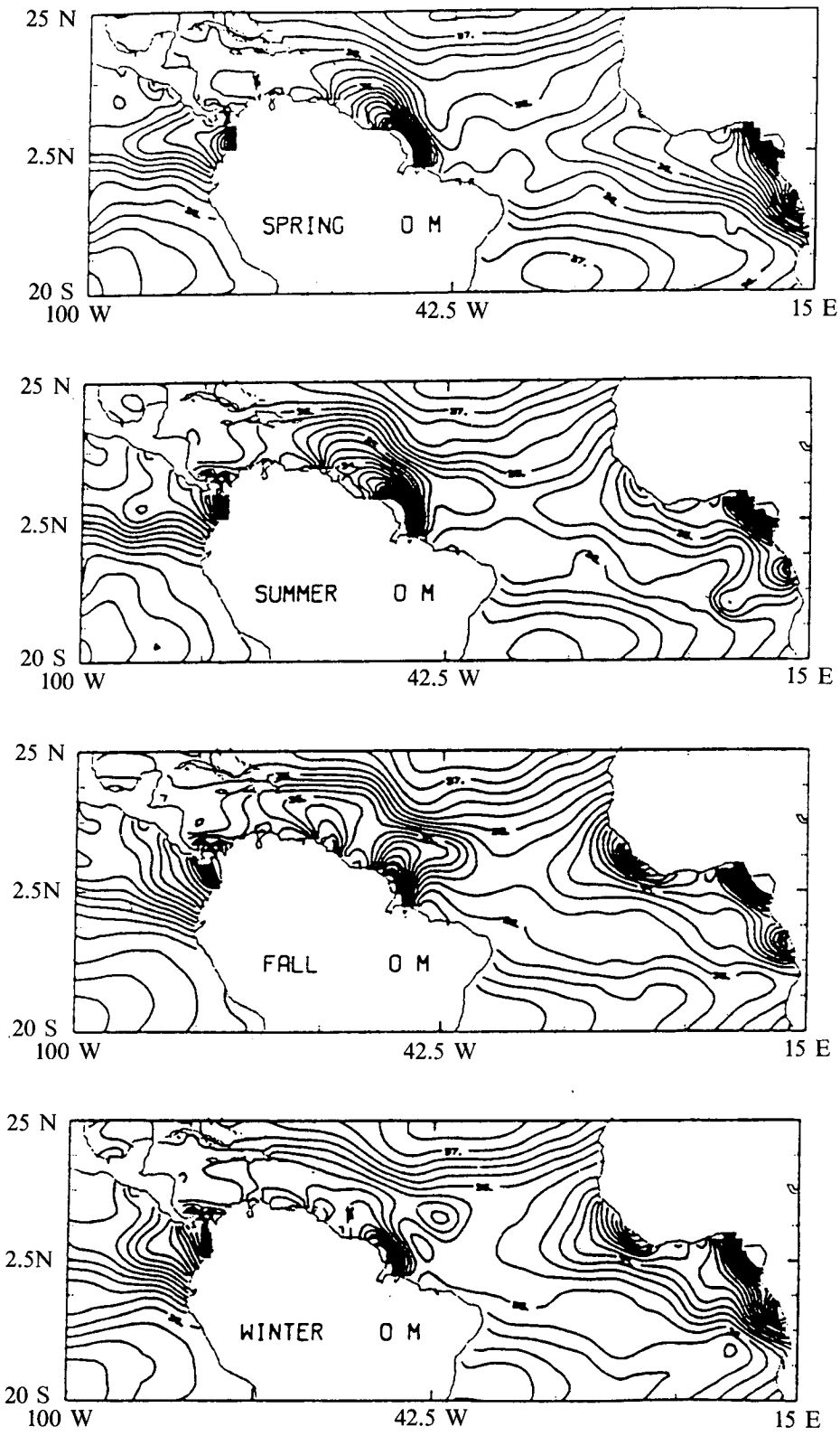

Figure III.3: Seasonal surface salinity variations in the tropical Atlantic (Yoo, 1990). The strongest changes occur in the western tropical Atlantic, associated with the Amazon outflow, and could be readily monitored by satellite.

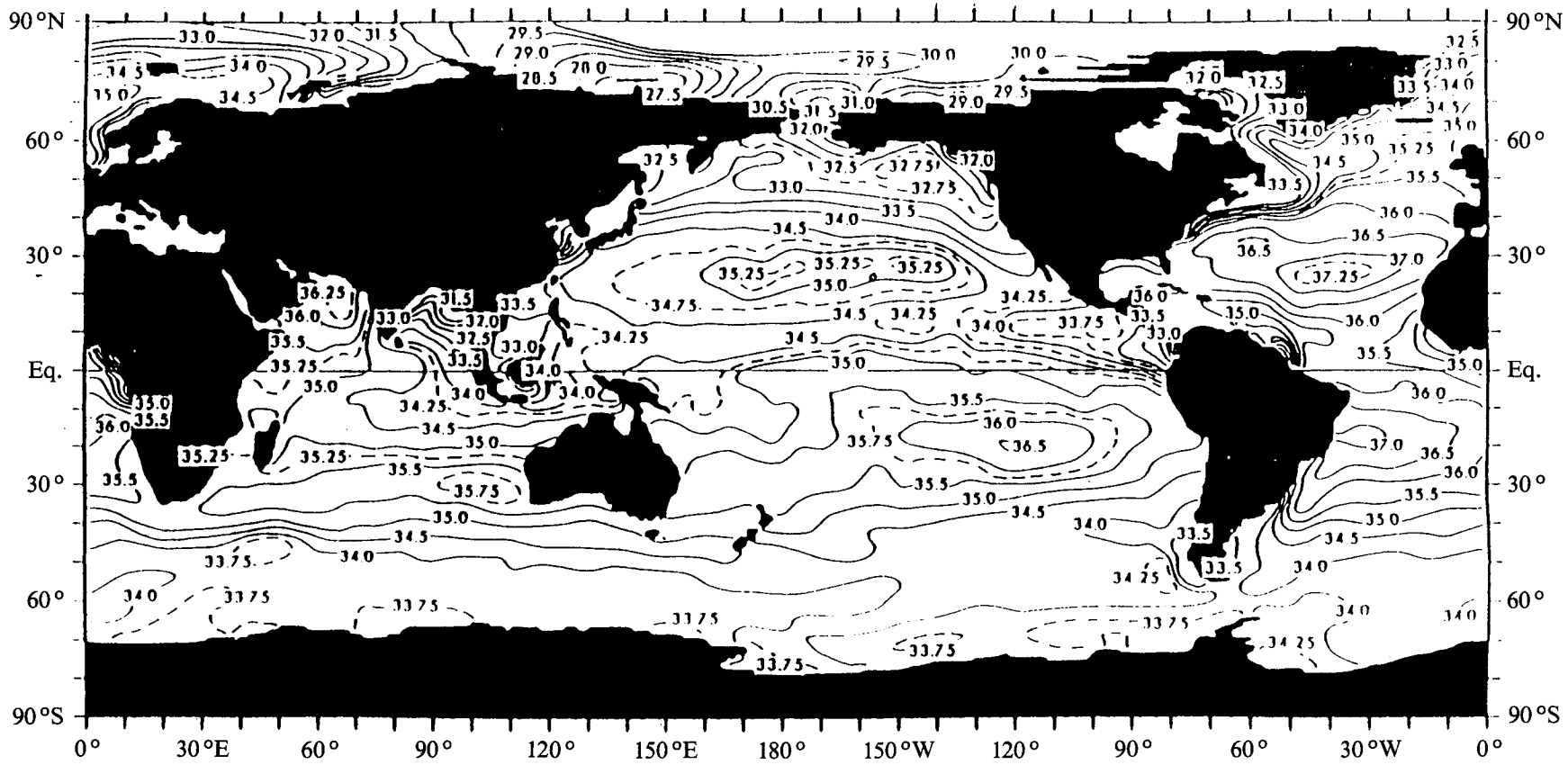

Figure III.4: The mean surface salinity field of the world ocean (Levitus, 1982), based on interpolation of all available surface observations. The data are actually very scarce; only 53 percent of the 1 degree latitude by 1 degree longitude squares have any samples. In contrast, a satellite sensor could provide about 1000 salinity samples per month in each 1 degree square. With a precision of about .05 to .1 parts per thousand it would be possible to monitor the annual and interannual variations of this global surface salinity field.

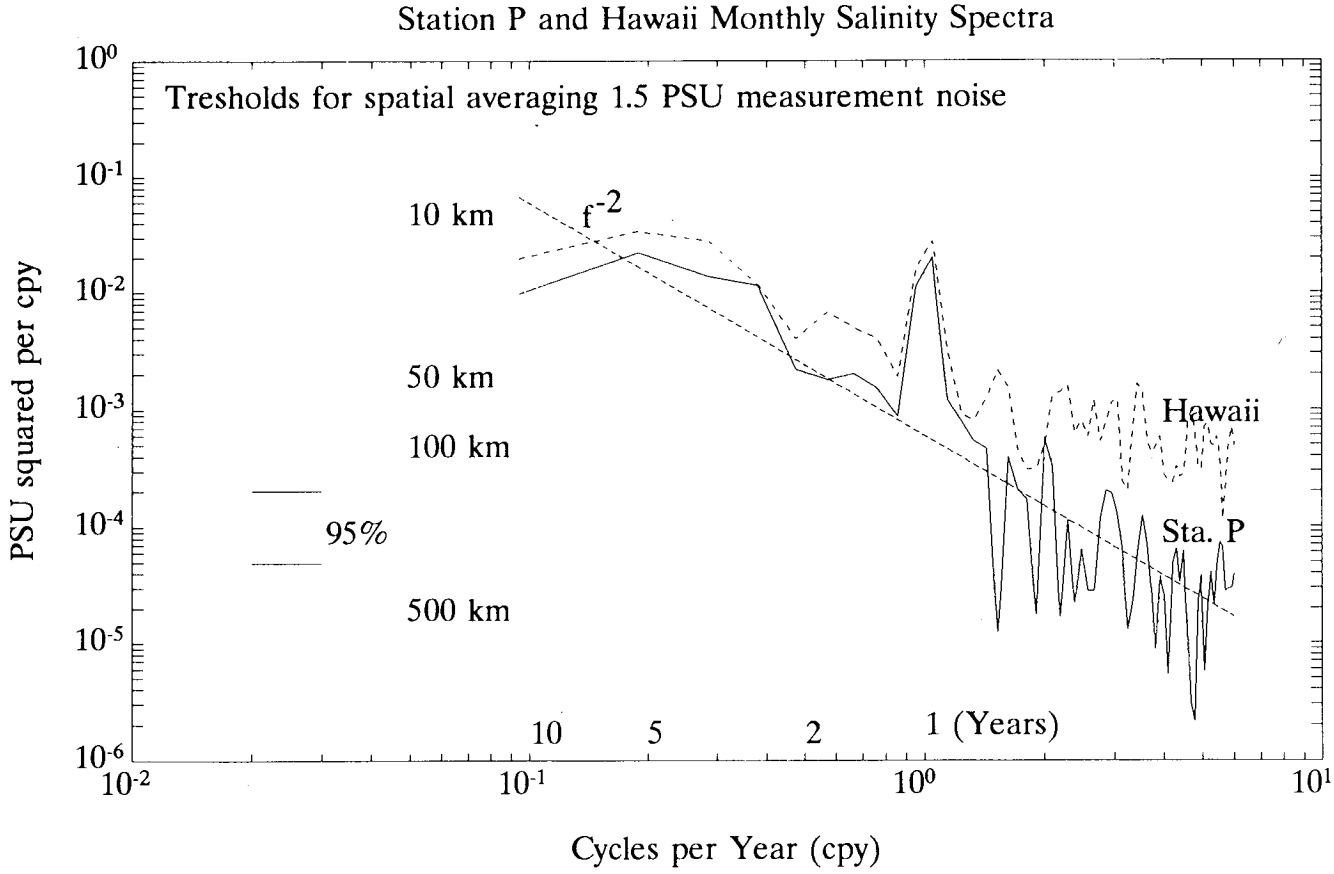

Figure III.5: Frequency spectra of two long (> 25 years) surface salinity time series from the North Pacific; Ocean Station Papa and Koko Head, Hawaii (data courtesy of S. Tabata and G. Broelert, respectively). Horizontal lines indicate the measurement white noise levels obtained by averaging the 10-km square samples over 50, 100 and 500 km.

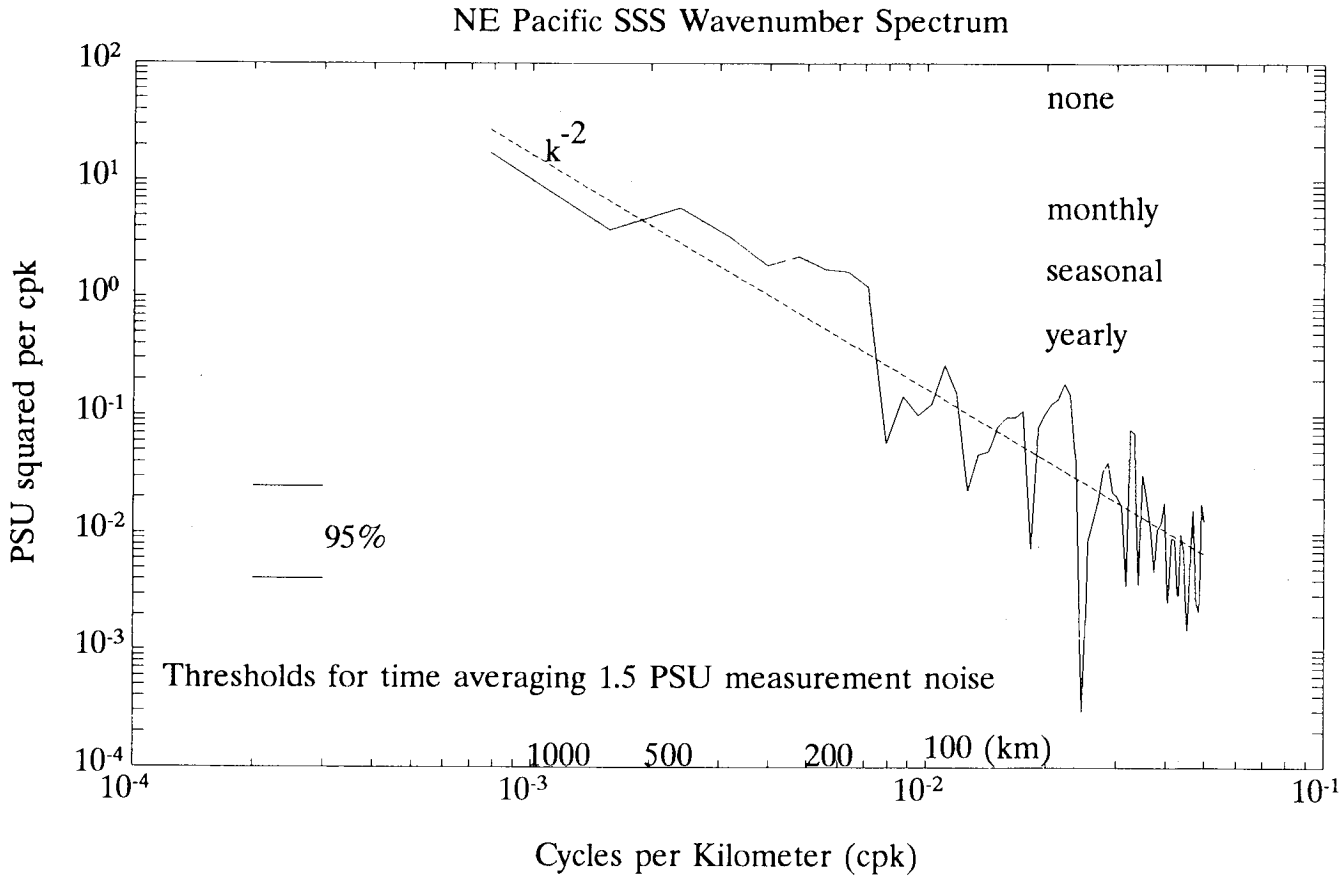

Figure III.6: Wavenumber spectrum of a trans-Pacific surface salinity survey from Alaska to Hawaii (data courtesy of T. Royer). Horizontal lines indicate the white noise levels for monthly, seasonal (3-month) and yearly time averaging intervals, assuming a 3-day sample interval. This indicates that for seasonal to yearly averages, surface salinity patterns of about 100 km and longer in length scale will be resolvable above the measurement noise.

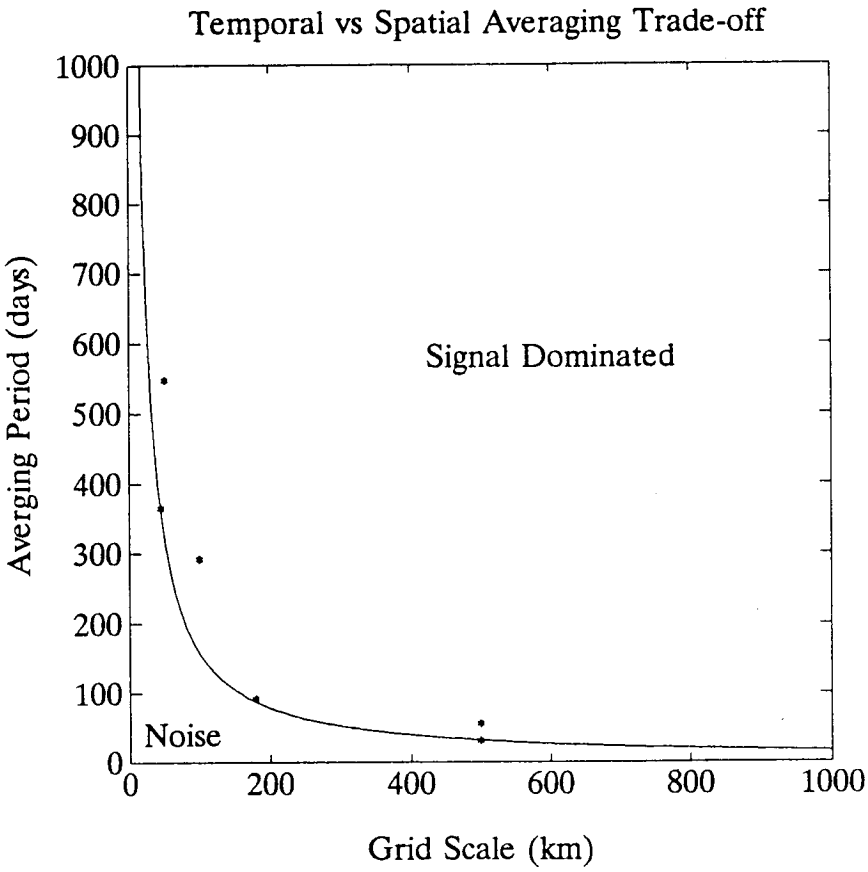

Figure III.7: An illustration of the trade-off between temporal and spatial averaging needed to determine the signal above the measurement noise. Resolution of shorter length scales requires averaging over longer timescales, and vice versa.

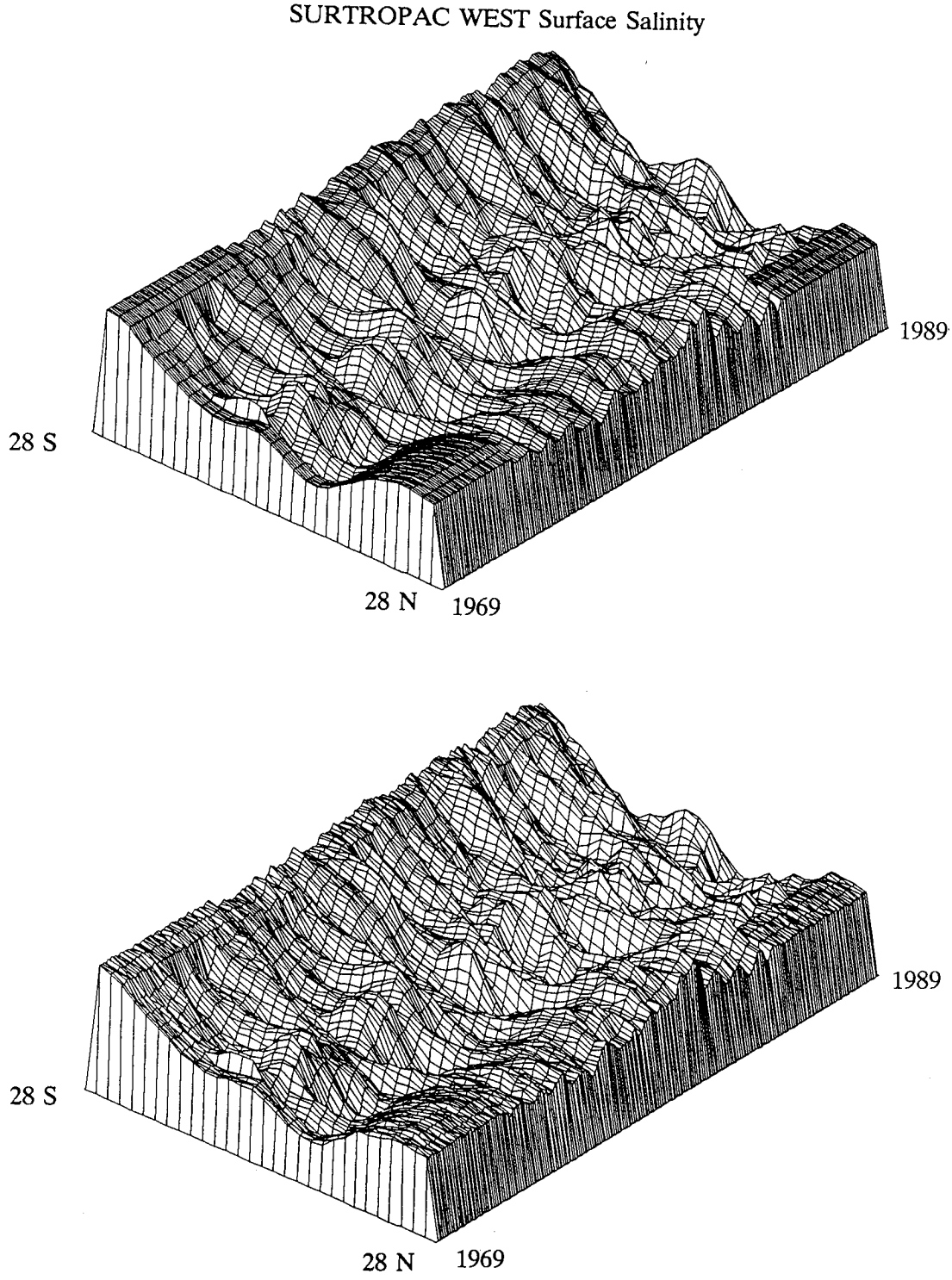

Figure III.8: (a) A surface contour plot of salinity variations along a meridional transect at 160° E longitude, between 28° S and 28° N latitude, from 1968 to 1988 (data courtesy of T. Delcroix). Data are monthly averages every 2 degrees of latitude. (b) Same as (a), except that measurement white noise for monthly and two degree latitude/longitude averages has been added.

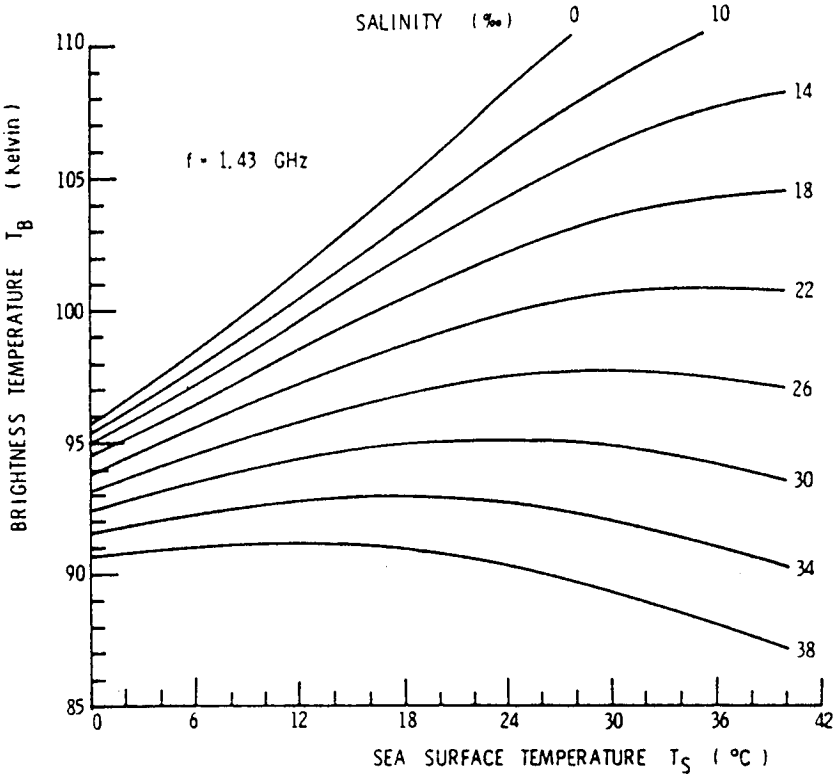

Figure III.9: The variation of brightness temperature (T_B) at nadir for a 1.4-GHz radiometer as a function of sea surface salinity and temperature (Swift and McIntosh, 1983). In principle, salinity can be found with independent measurements of T_B and surface temperature. However, the variation of T_B is small over the range of ocean salinities (32-37 ppt), with the greatest sensitivity at warmest temperature. Accurate salinity retrieval will place demanding accuracy requirements on a spaceborne radiometer.

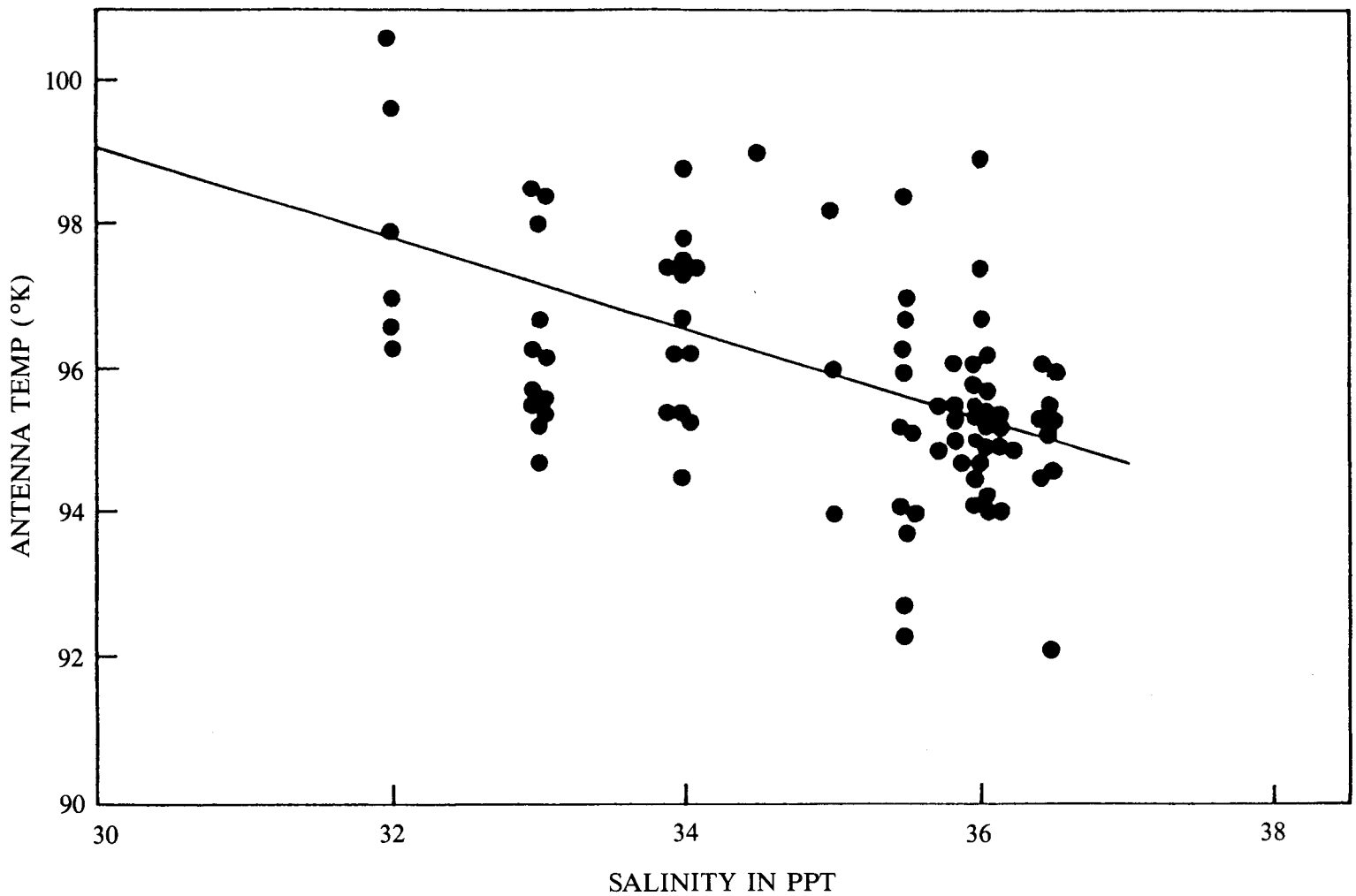

Figure III.10: Variation of brightness temperature with salinity, after correction for other effects, from the 1.4-GHz radiometer aboard Skylab in 1973 (Lerner and Hollinger, 1977). Surface salinity data were from general ocean climate atlases rather than simultaneous surface observation, and the radiometer did not have the higher precision of future systems.

IV. INSTRUMENT CONCEPT

A. INTRODUCTION

Conducting measurements at L band (1.4 GHz) from space requires placing relatively large, scanning antennas in orbit. Aperture synthesis, an interferometric technique in which the complex correlation of the output voltage from pairs of antennas is measured at many different baselines (Thompson, Moran and Swenson, 1988), offers a practical way of putting such structures in space. The concept of aperture synthesis was developed initially in radio astronomy to achieve high-resolution measurements. An example is the very large array (Napier *et al.*, 1983) which uses a "Y" configuration of elements to achieve the resolution of a filled array whose diameter is equal to that of the circle that encloses the "Y." Similar techniques can be applied to remote sensing from space to transform antenna complexity to signal processing complexity to obtain resolution that would not otherwise be achieved.

Space-based microwave observations for Earth science applications is a much younger discipline than radio astronomy. The first meaningful microwave observations of the Earth surface were not obtained until the Electronically Scanned Microwave Radiometer (ESMR) was launched on Nimbus 5 in 1972. The ESMR operated at a single frequency (19.3 GHz) and used a phased-array antenna to scan cross-track about nadir to produce an image of the Earth below it as the spacecraft advanced in orbit. Although its usefulness in geophysical applications was somewhat limited by the single frequency and the gross spatial resolution (50 km), the ESMR was soon used operationally by the Navy and Coast Guard to monitor the extent of sea ice in the north polar regions. Although much finer resolution is desirable, only microwave satellite systems can provide an economical means to monitor the polar regions because of cloud cover, darkness, and the harsh environment. The ESMR was superseded by the Scanning Multichannel Microwave Radiometer (SMMR) and the Special Sensor Microwave/Imager (SSM/I). The SMMR was launched on both Seasat I and Nimbus 7 in 1978, followed by the SSM/I in 1987. Both of these radiometer systems added dual polarization and multiple frequencies and provided more usable data to a diverse scientific community. The SMMR spanned 6.6 GHz to 37 GHz, and SSM/I spanned 18 GHz to 85 GHz. The spatial resolution of both instruments was of the same order as ESMR: that is, the aperture size has remained fixed for the last 20 years.

Spatial resolution has not improved and the size of the antenna has not exceeded 1 meter due to the impact of larger antennas on the size of spacecraft. In particular, a doubling of antenna size would require unrealistic antenna scanning rates for an imaging radiometer system. The problem is exacerbated by the low frequency (1.4 GHz) required for soil moisture and salinity measurements. At this frequency, large antennas are needed just to maintain existing resolution and large, mechanically scanned filled apertures are simply too costly to construct for space applications. Achieving increased resolution from space in a practical manner was the principal driver that motivated development of the synthetic aperture radiometer, ESTAR, originally proposed for EOS (Murphy *et al.*, 1987; Le Vine *et al.*, 1989).

B. BACKGROUND

The interferometer shown in Figure IV.1 is the basic building block of the aperture synthesis technique developed for Earth observations. If the outputs of the two isotropic antenna elements are multiplied together, it can be shown (e.g., Kraus, 1966) that the measurement is described by the following formula:

$$V(d) = \int_{-\pi/2}^{\pi/2} T_B(\theta) \exp[-j(2\pi d/\lambda)\sin(\theta)]\, d\theta \qquad (4)$$

where λ is the electromagnetic wavelength, θ is the incidence angle, and d is the spacing between elements. By making the change of variables $q = \sin(\theta)$, equation 4 can be cast in the form of a Fourier transform. Then V (d) can be treated as the spatial Fourier transform of the brightness temperature, $T_B(\theta)$, of the scene and the scene can then be reconstructed by performing the Fourier inverse.

The resolution of the measurement is determined by the range of d (i.e., by the total baseline) and not by the dimension of the antenna elements. Furthermore, if the scene is band limited, only values of V (d) at discrete samples of d are required for reconstruction of the scene.

To make measurements from space, aperture synthesis could be implemented in many ways (Le Vine, 1990). The problem is to achieve measurements at the available baselines within the limited time the spacecraft spends over the target. One way to achieve this is to use multiple interferometers (antenna pairs), each at a unique baseline. Since only one measurement is needed at each baseline, the resultant radiometer is very much thinned compared to a conventional antenna aperture.

C. NOISE PERFORMANCE AND CALIBRATION

The precision, ΔT, achievable with a synthetic aperture radiometer is given by

$$\Delta T = T_{sys} \sqrt{N/(B\tau)} \qquad (5)$$

where T_{sys} is the system noise temperature, B is the predetection bandwidth, τ is the post-detection integration time, and N is the number of wavelengths in the maximum baseline. (This result is applicable when the individual baselines are integer multiples of

$\lambda/2$ with no redundancies and the effective area of the individual antennas is proportional to $\lambda/2$.) The performance in this case is worse than that of a conventional total-power radiometer by the factor $\sqrt{N}$; however, a spacecraft sensor can be designed with performance that will be better than the 1 K required for the measurement of soil moisture. Further details on the noise performance are given in Ruf *et al.*, (1988) and Le Vine (1990).

In general, the ideal inversion of Equation 4, cannot be performed because of differences among the correlators. A practical inversion has been obtained (Le Vine *et al.*, 1992; A. Griffis, 1993) using a procedure that begins by approximating the integral with a sum. The result of the approximation is a set of algebraic equations that can be written in matrix notation in the following form:

$$V = C_o [GT] + V_b \qquad (6)$$

where V is a column matrix (1xM) whose entries are the output signals from the correlators, T is a column matrix (1xN) representing the system input (i.e., the brightness temperature of the scene, T_B), and G is an MxN matrix representing the "impulse response" of the system; C_o is an unknown scale factor and V_b is an offset. The impulse response, G, is the value of the integral in Equation 4 when the brightness temperature T_B is a delta function and values of G are measured by observing the response of the system to a noise source that is small compared to the resolution of the instrument. Given G, Equation 6 is inverted using a minimum least-squares inversion when $N > M$ (e.g., Cambell and Meys, 1979). In order to complete the inversion, the system constants C_o and V_b must be determined. This can be achieved by viewing two reference scenes with known brightness such as a lake or cold sky.

D. THE AIRCRAFT ESTAR

In order to demonstrate the utility of a thinned array radiometer for Earth observations, an airborne L-band prototype was developed at the University of Massachusetts and NASA/Goddard Space Flight Center, and flown several times on a NASA P-3 aircraft. A conceptual diagram is shown in Figure IV.2. The system uses five "stick" antennas, each consisting of a linear array of eight dipoles. The sticks provide resolution in the direction of aircraft motion, and resolution across track is obtained "synthetically" from the correlated output of pairs of sticks. This is a hybrid system that uses a "real" aperture along the aircraft direction of motion, and "synthetic" aperture in the cross-track direction.

The ESTAR was first test flown in June 1988 on a P-3 aircraft flown out of Wallops Island, VA. This first test flight was a mapping mission designed to determine whether this hybrid aperture synthesis concept would work when applied to Earth observations. To this end, lines were flown from the Atlantic Ocean over Virginia's Eastern Shore to the Chesapeake Bay. The purpose was to achieve a wide dynamic range of brightness temperatures to discriminate land from water, and then to detect more subtle changes associated with variations in soil moisture over the Eastern Shore. The flight was highly successful, considering the limited objectives of the mission. The L-band map, which clearly indicates both a response to soil moisture and the detection of land-water boundaries has recently been published (LeVine *et al.*, 1990). Subsequent analyses have also indicated that the ESTAR responds to more subtle signatures associated with differences in the emissivity of ocean and bay water due to differences in salinity.

Since these early experiments, the ESTAR instrument has been modified. It now has an improved antenna (better polarization characteristics), a new correlator, and repackaging to improve thermal control and permit the instrument to fly on the NASA C-130. These improvements have improved calibration and reduced processing artifacts. Recent validation experiments at the Walnut Gulch Watershed, Arizona in August 1991, gave excellent results (Le Vine *et al.*, 1992). An image obtained during these flights is shown in Figure II.5.

E. A SPACECRAFT CONCEPT OF A THINNED ARRAY MICROWAVE RADIOMETER

A preliminary study of a candidate spacecraft instrument to measure soil moisture has been undertaken using a thinned array radiometer of the aircraft ESTAR design (i.e., using aperture synthesis in one dimension). The concept described here is the result of cooperative work between the University of Massachusetts, the Goddard Space Flight Center, the Langley Research Center and the Jet Propulsion Laboratory. The system would be deployed in a sun-synchronous orbit (to provide measurements at the same time of day) and have a revisit time of 3 days, a frequency consistent with the soil moisture measurement requirements (Murphy *et al.*, 1987). Choosing an orbit at an altitude of about 350 km, an instrument swath width of ±40° and a synthesized antenna beam with a half-power beamwidth of 1.66° at nadir, results in coverage of 95% of the Earth and a resolution cell at nadir of 8 km x 10 km.

Conceptual drawings of a system which meets these requirements are shown in Figures IV.3 and IV.4. The antennas are slotted waveguides. The prime frequency is 1.4 GHz, which requires slotted waveguide antennas 9.4 meters in length. In order to enhance the capability of the system, additional thinned array radiometers operating at 2.65 GHz and 5.0 GHz have been nested within the L-band array in order to provide secondary channels to correct for effects due to the vegetation canopy and possibly to estimate soil moisture profile. Over water the L- and S-band channels together provide an estimate of ocean salinity and temperature (Blume et al., 1978; Swift and McIntosh, 1983), with the C-band channel providing ancillary information such as ocean-surface windspeed. The S- and C-band sticks are proportionately shorter because of the higher operating frequencies.

Engineering performance specifications are given in Table I. The instrument has 14 stick antennas at each of the three operating frequencies. Each antenna element is a slotted waveguide 44.8 wavelengths long. The elements are positioned along the direction of the spacecraft velocity vector, so that their fan-beam antennas overlap cross-track to the direction of spacecraft motion. The placement of antenna elements follows the minimum redundancy linear array configuration described in Ruf *et al.*, (1988). Images are formed by cross-correlating all possible pairs of antennas, and then converting these correlation measurements to image pixels in software. This process produces simultaneous synthesized narrow antenna beams at all frequencies and in all directions cross-track to the direction of motion. These synthesized antenna beams are equivalent to those which would be produced by a conventional multibeam phased-array antenna. If the cross-track resolution were to be achieved using a conventional phased-array antenna, approximately 100 individual sticks would be needed at each frequency, and it would be difficult to accommodate such a large mass within the shroud of a single Delta-II class of launch vehicle. By using aperture synthesis only 14 sticks are required for each channel, and adequate empty space is available within the L-band array to nest in the higher frequencies.

In the proposed instrument the sticks would be made of standard waveguide, and the entire structure would be folded, accordion style, to fit into the shroud of a Delta-II class launch vehicle. The shroud could accommodate all the sticks without folds except at L-band, and these would have to be folded once near their midpoint (indicated by the hinge line, Figure IV.3). The deployment and support structure is composed of tubular truss similar to structures that have been successfully designed in the past. Assuming existing composite graphite/epoxy designs, each waveguide element would weigh about 5.5 kg (L-band), 1.5 kg (S-band), and 0.5 kb (C-band) for an antenna total of about 105 kg. Estimates of the total weight of the instrument, supporting structure and spacecraft are well below the capacity of a Delta-II class launch vehicle.

Such an array would provide resolution at nadir of about 10 km. Assuming an integration time of 1 s, a bandwidth of 10 MHz and a system noise temperature of 500 K, one would achieve a sensitivity of better than 1 K, which is adequate for the soil moisture measurement. The sensitivity needed for the salinity measurement (about .02 K) could be obtained by averaging over adjacent pixels and time as described in Section III, above.

Table1. ESTAR Engineering Performance Specification

ORBIT SPECIFICATIONS

Altitude (km)	350
Sun-synchronous orbit repeat (days)	3
Cross-track swath width (km)	± 600
Earth coverage (%)	≥95

INSTRUMENT SPECIFICATIONS

Antenna Array element count	14 @ each frequency
Antenna Array element type	44.8λ slotted waveguide
Nadir along-track HPBW (deg)	1.66
Nadir cross-track HPBW (deg)	1.28
Nadir footprint (km)	7.8 x 10.2
Total Instrument Weight (kg)	341
Total Instrument Power (W)	157
Launch Size Envelope	Delta II payload
On-orbit Deployed Size (m)	9.5 x 9.5 antenna array
	1.0 x 1.0 electronics
Receiver Noise Temperature (K)	150 @ 1.4 GHz
	200 @ 2.7 GHz
	250 @ 5.0 GHz
Pre-detection BW (MHz)	27 @ 1.4 GHz
	37 @ 2.7 GHz
	48 @ 5.0 GHz
Post-detection integration time (s)	0.7
Image Measurement Precision, ΔT (K)	0.5 @ each frequency
Image Calibration Accuracy (K)	1.0

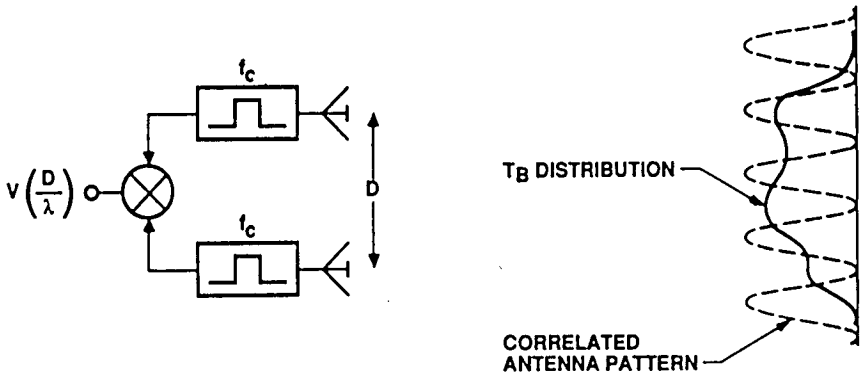

Figure IV.1: Conceptual diagram of a two-element imaging microwave interferometer.

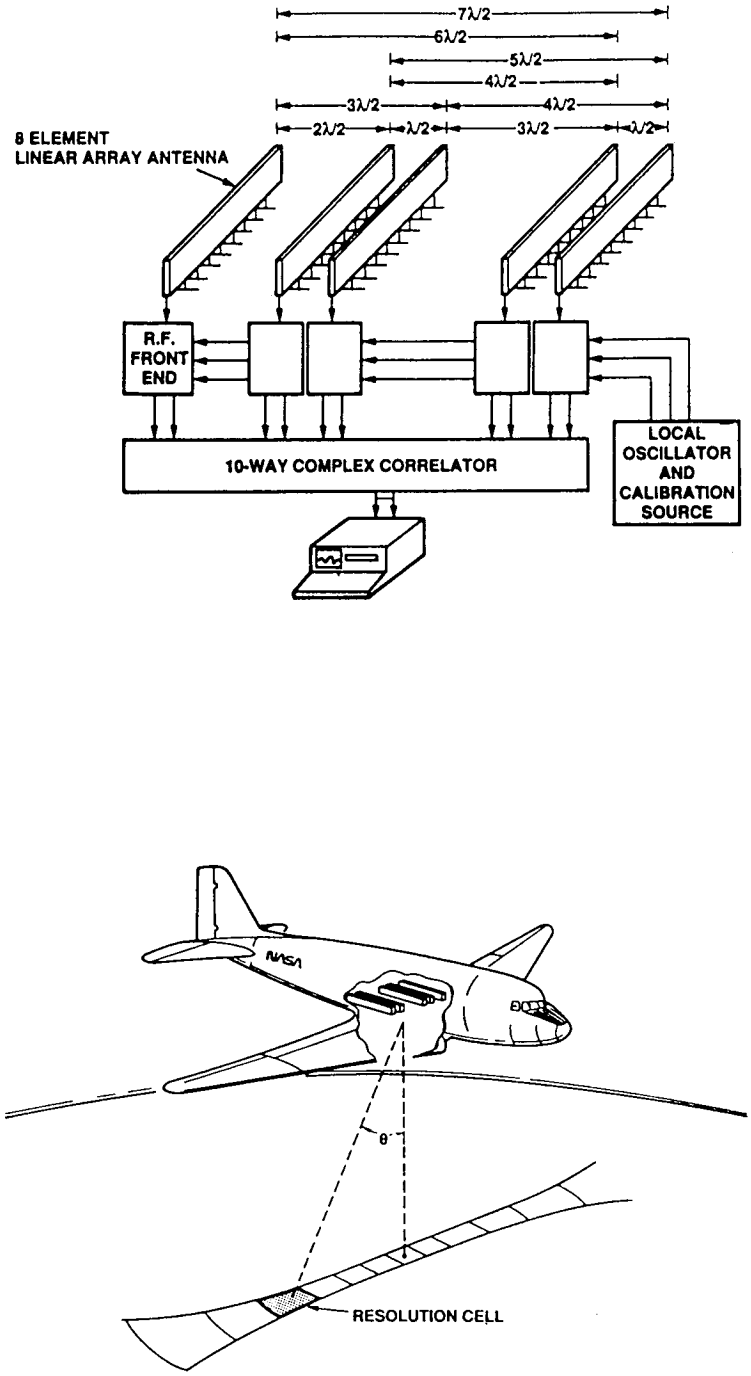

Figure IV.2: (top) Block diagram of the ESTAR prototype; (bottom) Configuration of the aircraft prototype.

OVERVIEW:

- THREE CHANNELS (1.41, 2.65, 5.00 GHz)
- 14 SLOTTED WAVEGUIDE ANTENNA ELEMENTS PER CHANNEL
- APERTURE SIZE = 44.8λ × 44.8λ AT ALL FREQUENCIES

ANTENNA ARRAY ELEMENTS:

FREQUENCY (GHz)	1.41	2.65	5.00
LENGTH (cm)	950.8	505.9	268.1
CROSS SECTION	STANDARD WAVEGUIDE		
WEIGHT (kg/ELEMENT)	6.6	1.5	0.5

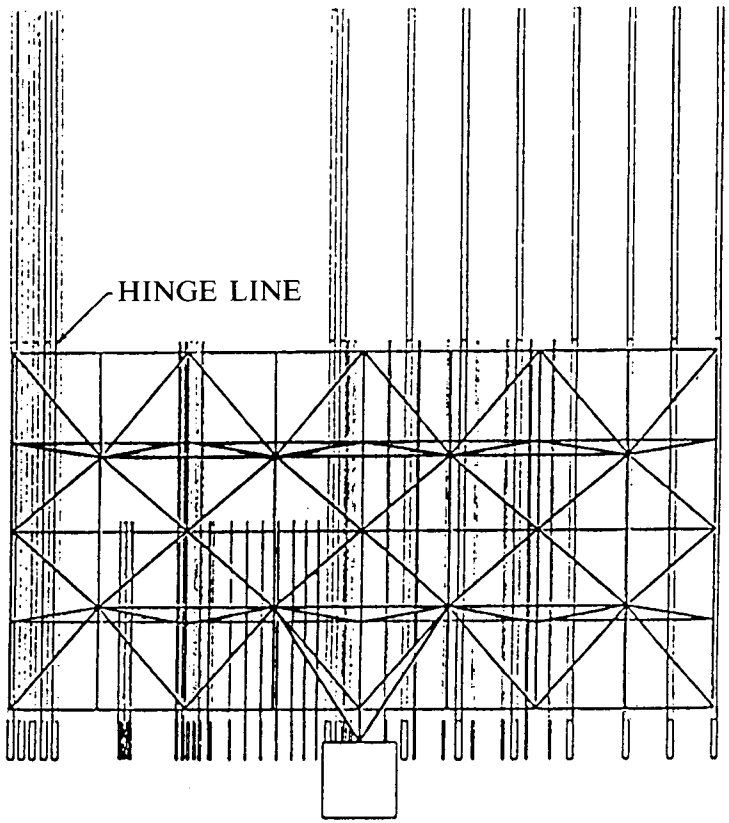

Figure IV.3: Instrument to measure soil moisture and ocean salinity from space.

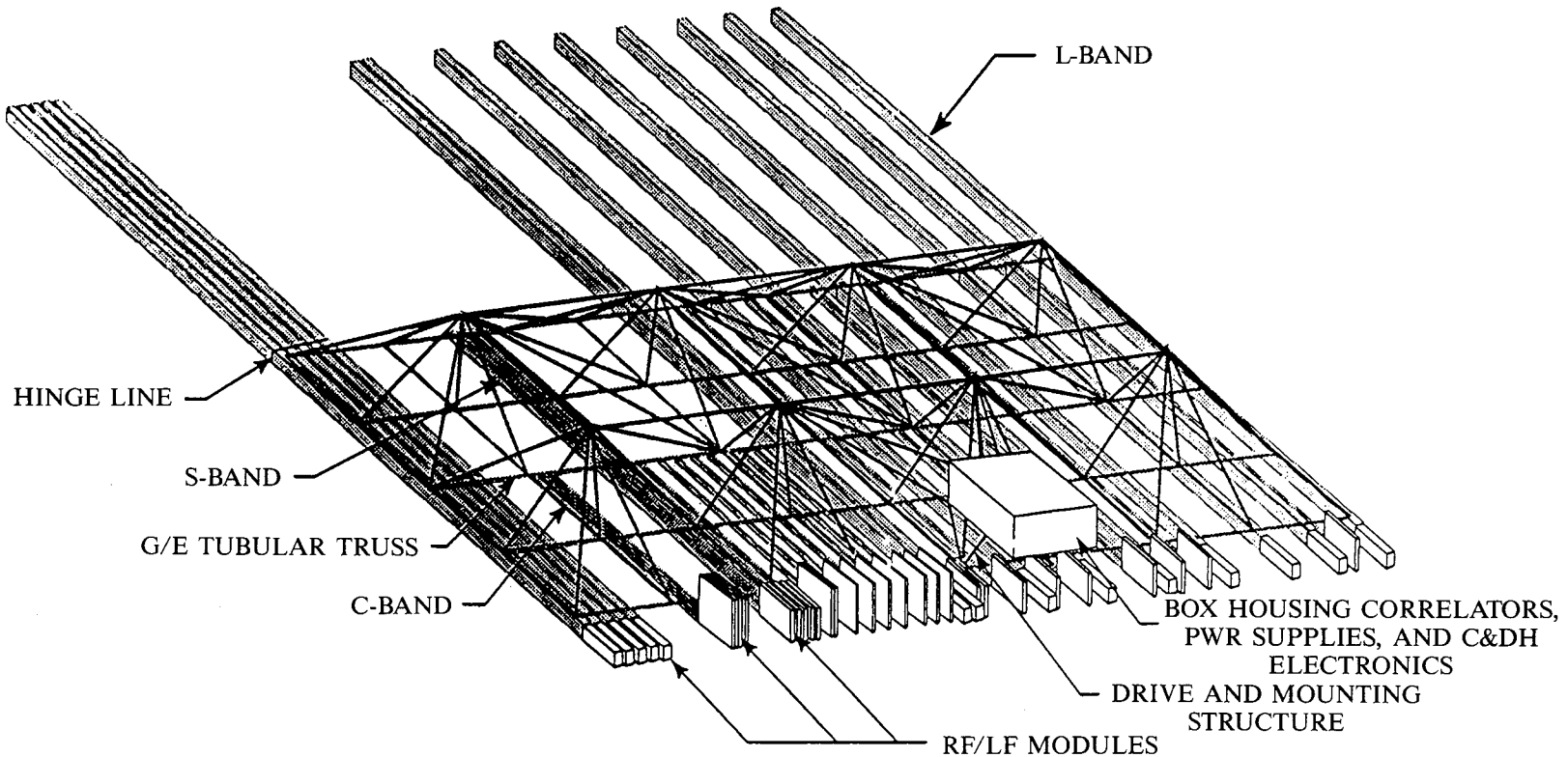

Figure IV.4: Perspective view of the instrument in Figure 3 with the deployment truss shown.

V. REFERENCES

Abramopoulos, C. Rosenzweig, and B. Choudhury, (1988) "Improved ground hydrology calculations for global climate models (GCMs): soil water movement and evapotranspiration," *Journal of Climate*, 1, No. 9, 921-941.

Andre, J.C., J.P. Goutorbe, and A. Perrier, (1986) "Hapex-Mobilhy: A hydrologic atmospheric experiment for the study of water budget and evaporation flux at the climate scale," *Bull. Amer. Met. Soc.*, 67, 138-144.

Avissar, R. and R.A. Pielke, (1989) "A parameterization of heterogeneous land surface for atmospheric numerical models and its impact on regional meteorology," *Mon. Wea. Rev.*, 117, 2113-2136.

Avissar, R., (1990) "A statistical-dynamical approach to parameterize subgrid-scale land-surface heterogeneity in climate models," Land Surface-Atmospheric Interactions for Climate Models: Observations, Models, and Analyses, ed. by Eric F. Wood, Kluwer Academic Publishers.

Blanchard, B.J., McFarland, M.J., Schmugge, T.J., Rhoades, E. (1981) "Estimation of soil moisture with API algorithms and microwave emission," Water Resources Bulletin 17:767-774.

Blume, H-J.C., B.M. Kendall and J.C. Fedors, 1978, "Measurement of Ocean Temperature and Salinity via Microwave Radiometry," *Boundary-Layer Meteorol.*, Vol. 13, 295-380.

Blume, H.C., B.M. Kendall, 1982, "Passive microwave measurements of temperature and salinity in coastal zones," IEEE Trans. Geosci. Rem. Sens., GE-20, 394-404.

Broecker, W.S., 1991, "The great ocean conveyor," Oceanography, 4, 79-89.

Broecker, W.S. and J.P. Kennett, 1989, "The routing of Laurentide ice-sheet meltwater during the Younger Dryas cold event," it Nature 341:318-321.

Cambell, S.L. and C.D. Meys (1979), Generalized Inverse of Linear Transformations, Dover, New York, Chapter 2.

Charney, J., W. Quirk, S. Chow and J. Kornfield, (1977) "A comparative study of the effects of albedo change on drought in semi-arid regions," *J. Atmos. Sci.*, 34, 1366-1385.

Choudhury, B.J. and Golus, R.E. (1988) "Estimating soil wetness using satellite data," *Int. J. of Remote Sensing*, 9:1251-1257.

Delcroix, T. and F. Masia, 1989, "Atlas of sea surface temperature and salinity variations in the tropical Pacific (1969-1988)", Rapport scientifiques et techniques, Sciences de la mer, *Oceanographie physique*, No. 2, ORSTOM, Centre de Noumea, New Caledonia.

Delworth, T.L., and S. Manabe, (1988) "The influence of potential evaporation on the variabilities of simulated soil wetness and climate," *Journal of Climate*, 1, No. 5.

Delworth, T.L., and S. Manabe, (1989) "The influence of soil wetness on near-surface atmospheric variability," *Journal of Climate*, 2, No. 12, 1447-1462.

Dickinson, R.E., A Henderson-Sellers, P.J. Kennedy, M.F. Wilson, (1986) "Biosphere-atmosphere transfer scheme (BATS) for the NCAR community climate model," NCAR Technical Note, 69 pp.

Dickson, R. R., J. Meincke, S.-A. Malmberg and A. J. Lee, 1988, "The `Great Salinity Anomaly' in the northern North Atlantic 1968-1982," *Prog. Oceanogr.* 20, 103-151.

Dlugi, R. "Chemical Reactions and Transport Processes within and above Vegetation," presented at the European Geophysical Society Meeting, April 22 - 26, 1991, Wiesbaden, Germany.

Donsguy, J.R., 1987, "Recent advances in the knowledge of the climatic variations in the tropical Pacific Ocean," *Prog. Oceanogr.*, 19,49-85.

Eagleman, J.R. and Lin, W.C. (1976) "Remote sensing of soil moisture by a 21 cm passive radiometer," *J. Geophys. Res.* 81:3660-3666.

Engman, E.T. (1992), "Soil Moisture Needs in Earth Sciences," IGARSS-92, 477-479, Houston, TX, May 1992.

Entekhabi, D. and P.S. Eagleson, (1989) "Land surface hydrology parameterization for atmospheric general circulation models including subgrid scale spatial variability," *Journal of Climate*, 2, 816-831.

Famiglietti, J.S., and E.F. Wood, (1990) "Evapotranspiration and runoff from large land areas: land surface hydrology for atmospheric general circulation models," in Land Surface-Atmospheric Interactions for Climate Models: Observations, Models, and Analyses, ed. by Eric F. Wood, Kluwer Academic Publishers.

Griffis, A. (1993), "Earth Remote Sensing with an Electronically Scanned Thinned Array Radiometer," Dissertation,

University of Massachusetts, February, 1993.

Harrington, R.F. and R.W. Lawrence (1985), "An Airborne Multibeam 1.4 GHz Pushbroom Microwave Radiometer," *Proc. Int. Geosci & Remote Sensing Sym.* (IGARSS), pp 601-606.

Heymsfield, G.M. and Fulton, R. (1992) "Modulation of SSM/I microwave soil radiances by rainfall," *Remote Sensing of Environment*, 37:187-202.

Jackson, T.J. Schmugge, T.J., and Wang, J.R. (1982) "Passive microwave sensing of soil moisture under vegetation canopies," *Water Resources Research*, 18:1137-1142.

Jackson, T.J., Schmugge, T.J., and O'Neill, P.E. (1984) "Passive microwave remote sensing of soil moisture from an aircraft platform," *Remote Sensing of Environment*, 14:135-142.

Kerr, Y.H. and Njoku, E.G. (1990) "A semiempirical model for interpreting microwave emission from semiarid land surfaces as seen from space," *IEEE Trans. on Geoscience and Remote Sensing*, GE-28:384-393.

Klein, L.A. and C.T. Swift, 1977, "An Improved Model for the Dielectric Constant of Sea Water at Microwave Frequencies," *IEEE Trans. Antennas and Prop.*, aP-25 (#1), 104-111.

Kraus, J.D. (1966), Radio Astronomy, McGraw-Hill Book Company, chapter 6.

Lagerloef, G.S.E., C.T. Swift, D.M. Le Vine and A. Griffis, 1992, "Remote Sensing of Sea Surface Salinity: Airborne and Satellite Concepts," AGU Ocean Sciences Meeting, New Orleans, LA, January.

Lakshmi, V. and Eric F. Wood, (1991) "Spatial Temporal Variability and Scaling Using a Biophysical Land-Atmospheric Model," Paper H41A-9, Eos, Transactions of the American Geophysical Union, 72(17), pp 122, April 23.

Lazier, J., 1980, "Oceanic conditions at Ocean Weather Ship BRAVO;1964-1974," *Atmos.- Ocean*, 18:227-238.

Lazier, J., 1988, "Temperature and Salinity changes in the Deep Labrador Sea, 1962-1986," *Deep Sea Res.*, Vol 3-5, pg 1247.

Lerner, R.M. and J.P. Hollinger, 1977, "Analysis of 1.4 GHz Radiometric Measurements from Skylab," *Remote Sensing Environment*, Vol 6, pp 251-269.

Le Vine, D.M., M. Kao, A.B. Tanner, C.T. Swift and A. Griffis, 1990, "Initial Results in the Development of a Synthetic Aperture Radiometer," *IEEE Trans Geosci. & Remote Sensing*, Vol. 28 (4), 614-619.

Le Vine, D.M., T. T. Wilheit, R. Murphy and C. Swift, 1989, "A Multifrequency Microwave Radiometer of the Future," *IEEE Trans. on Geosci & Remote Sensing*, 27 (2), 193-199.

Le Vine, D.M. (1990), "The Sensitivity of Correlation Radiometers for Remote Sensing from Space," *Radio Science*, Vol. 35 (4), pp 441-453, July.

Le Vine, D.M., A. Griffis, C.T. Swift and T.J. Jackson (1992), "ESTAR: A Synthetic Aperture Microwave Radiometer for Measuring Soil Moisture," IGARSS-92, Vol. II, pp 1755-1757, Houston, TX, May, 1992.

Levitus, S., 1982, "Climatological Atlas of the World Ocean," NOAA, U.S. Dept. of Commerce, Washington D.C., 173 pp.

Manabe, S., J. Smagorinsky and R.J. Strickler, (1965) "Simulated climatology of a general circulation model with a hydrological cycle," *Mon. Wea. Rev.*, 93, 769-798.

Manabe, S. (1969) "Climate and the Ocean Circulation I The Atmospheric Circulation and the Hydrology of the Earth's Surface," *Mon. Wes. Rev.* vol. 97 pp 739.

McFarland, M.J. (1976) "The correlation of Skylab L-band brightness temperature with antecedent precipitation," in preprint of Conf. Hydrometeorology (Fort Worth, TX), AMS, 60-65.

Murphy, R. et al., 1987, "Earth Observing System Report," Vol. IIe, "High-Resolution Multifrequency Microwave Radiometer Instrument (HMMR)," Instrument Panel Report, National Aeronautics and Space Administration, Washington, D.C.

Napier, P.J., A.R. Thompson and R.D. Ekers (1983), "The Very Large Array: Design and Performance of a Modern Synthesis Radio Telescope," Proceedings IEEE, Vol 71 (11), pp 1295-1320.

Oglesby, R.J. and D.J. Erikson (1989) "Soil Moisture and Persistence of North American Drought," *Journal of Climate*, 2, 1362-1380.

Pampaloni, P., Paloscia, S., Chiarantini, L., Coppo, P., Gagliani, S., and Luzi, G. (1990) "Sampling depth of soil moisture content by radiometric measurement at 21 cm wavelength: some experimental results," *Int. J. of Remote Sensing*, 11:1085-1092.

Rango, A. *et al.* (1980), "Plan of Research for Integrated Soil Moisture Studies," Recommendations of the Soil Moisture Working Group, National Aeronautics and Space Administration, Washington, D.C., 70pp.

Rind, D., (1982) "The influence of ground moisture conditions in North America on summer climate as modeled in the GISS GCM," *Mon. Wea. Rev.*, 110, 1487-1494.

Rowntree, P.R., and J.R. Bolton, (1983) "Simulation of the atmospheric response to soil moisture anomalies over Europe," *Quart. J. Roy. Meteor. Soc.*, 109, 501-526.

Ruf, C.S., C.T. Swift, A.B. Tanner and D.M. Le Vine (1988), "Interferometric Synthetic Aperture Microwave Radiometry for the Remote Sensing of the Earth," *IEEE Trans. Geosci & Remote Sensing*, Vol. 26 (5), pp. 597-611.

Schmugge, T.J., Menennly, J.M., Rango, A., Neff, R. (1977) "Satellite microwave observations of soil moisture variations," *Water Resources Bulletin* 13:265-281.

Schmugge, T.J., Wang, J.R., and Asrar, G. (1988) "Results from the pushbroom microwave radiometer flights over the Konza Prairie in 1985," *IEEE Tran. on Geoscience and Remote Sensing*, GE-26:590-596.

Schmugge, T., Jackson, T.J., Kustas, W.P., and Wang, J.R. (1992) "Passive microwave remote sensing of soil moisture: results from HAPEX, FIFE and MONSOON '90," *ISPRS Journal of Photogrammetry and Remote Sensing*, 47:127-143.

Sellers, P.J., and J.L. Dorman, (1987) "Testing the simple biosphere model (SiB) using point micrometereological and biophysical data," *Journal of Climate and Applied Meteorology*, 26 622-651.

Sellers, P.J., Y. Mintz, Y.C. Sud, and A. Dalcher, (1986) "A simple biosphere model (SiB) for use within general circulation models," *Journal of the Atmospheric Sciences*, 43, No. 6.

Sellers, P.J., F.G. Hall, G. Asrar, D.E. Strebel, and R.E. Murphy, (1988) "The First ISLSCP Field Experiment (FIFE)," *Bulletin of the American Meteorological Society*, 69, 22-27.

Sellers, P.J., W.J. Shuttleworth, J.L. Dorman, A. Dalcher, and J.M. Roberts, (1989) "Calibrating the simple biosphere model for amazonian tropical forest using field and remote sensing data. Part I: Average calibration with field data," *Journal of Applied Meteorology*, 28, No. 8, 727-759.

Shukla, J., and Y. Mintz, (1982) "The influence of land-surface evapotranspiration on earth's climate," *Science*, 215, 1498-1501.

Shutko, A.M., (1986) "Microwave radiometry of water surface and grounds," Publishing House "Nauka," Moscow, USSR, p. 192 (English translation).

Shuttleworth, W.J., (1990) "Insight from large-scale observational studies of land/atmosphere interactions," Land Surface-Atmospheric Interactions for Climate Models: Observations, Models, and Analysis, ed. by Eric F. Wood, Kluwer Academic Publishers.

Swift, C.T., D.M. Le Vine and C.S. Ruf (1991), "Aperture Synthesis Concepts in Microwave Remote Sensing of the Earth," IEEE Trans. MTT, Vol. 39 (12), 1931-1935.

Swift, C.T. and R.E. McIntosh, 1983, "Considerations for microwave remote sensing of ocean-surface salinity," *IEEE Trans. Geosci. Rem. Sens.*, GE-21, 480-491.

Swift, C.T., 1980, "Passive Microwave Remote Sensing of the Ocean - A Review," *Boundary-Layer Meteorol.*, 18, pp 25-54.

Thomann, G.C., 1976, "Experimental Results of the Remote Sensing of Sea-Surface Salinity at 21-cm Wavelength," *IEEE Trans. Geosci. Electronics*, GE-14, pp 198-214.

Thompson, A.R., J.M. Moran and G.W. Swenson (1988), Interferometry and Synthesis in Radio Astronomy, J. Wiley & Sons, New York.

Walker, J.M. and P.R. Rowntree, (1977) "The effect of soil moisture on circulation and rainfall in a tropical model," *Quart. J.R. Meteor. Soc.*, 103, 29-46.

Walsh, J. E., and W. L. Chapman, 1990, "Arctic Contribution to upper ocean variability in the North Atlantic," *Jour of Climate*, vol 3(12): 1462-1473.

Wang, J.R. (1985) "Effect of vegetation on soil moisture sensing observed from orbiting microwave radiometers," *Remote Sensing of Environment*, 17:141-151.

Wang, J.R., Shiue, J.C., Schmugge, T.J., and Engman, E.T. (1990) "The L-band PBMR measurements of surface soil moisture in FIFE," *IEEE Trans. on Geoscience and Remote Sensing* GE-28:906-913.

Wetzel, P.J. and J-T. Chang, (1986) "Concerning the relationship between evapotranspiration and soil moisture," *Journal of Climate and Applied Meteorology*, 26, 18-27.

Wetzel, P.J. and J-T. Chang, (1988) "Evapotranspiration from nonuniform surfaces: a first approach for short-term numerical weather prediction," *Mon. Wea. Rev.* 116, 600-621.

Wilson, M.J., A. Henderson-Sellers, R.E. Dickinson and P.J. Kennedy, (1987) "Sensitivity of the biosphere-atmosphere transfer scheme (BATS) to the inclusion of variable soil characteristics," *Journal of Climate and Applied Meteorology*, 26, No. 3, 341-362.

Yoo, J.-M., and J.A. Carton, 1990, "Annual and interannual variations of the freshwater budget in the tropical Atlantic Ocean and Caribbean Sea," *J. Phys. Oceanogra.*, 20, 831-845.

Yoo, J-M., 1990, "Seasonal freshwater and salinity budgets in the tropical Atlantic Ocean," Ph.D. Dissertation, University of Maryland, College Park, MD, 185pp.

REPORT DOCUMENTATION PAGE

Form Approved
OMB No. 0704-0188

1. AGENCY USE ONLY *(Leave blank)*	2. REPORT DATE	3. REPORT TYPE AND DATES COVERED
	July 1993	Technical Memorandum

4. TITLE AND SUBTITLE
ESTAR—The Electronically Scanned Thinned Array Radiometer for Remote Sensing Measurement of Soil Moisture and Ocean Salinity

5. FUNDING NUMBERS
Code 975

6. AUTHOR(S)
C. T. Swift, Chairman

7. PERFORMING ORGANIZATION NAME(S) AND ADDRESS(ES)
Goddard Space Flight Center
Greenbelt, Maryland 20771

8. PERFORMING ORGANIZATION REPORT NUMBER
93B00074

9. SPONSORING/MONITORING AGENCY NAME(S) AND ADDRESS(ES)
National Aeronautics and Space Administration
Washington, D.C. 20546–0001

10. SPONSORING/MONITORING AGENCY REPORT NUMBER
TM–4523

11. SUPPLEMENTARY NOTES
ESTAR Working Group: C. T. Swift, D. M. Le Vine, J. A. Carton, D. B. Chelton, E. T. Engman, A. Gordon, T. J. Jackson, G. S. E. Lagerloef, E. Njoku, I. Rodrigues–Iturbe, C. S. Ruf, S. Sarooshian, T. J. Schmugge, and R. A. Weller

12a. DISTRIBUTION/AVAILABILITY STATEMENT
Unclassified–Unlimited
Subject Category 43
Report available from the NASA Center for AeroSpace Information, 800 Elkridge Landing Road, Linthicum Heights, MD 21090; (301) 621–0390.

12b. DISTRIBUTION CODE

13. ABSTRACT *(Maximum 200 words)*

This report is the product of a working group assembled to help define the science objectives and measurement requirements of a spaceborne L–band microwave radiometer devoted to remote sensing of surface soil moisture and sea surface salinity. Remote sensing in this long–wavelength portion of the microwave spectrum requires large antennas in low–Earth orbit to achieve acceptable spatial resolution. The proposed radiometer, ESTAR, is unique in that it employs aperture synthesis to reduce the antenna area requirements for a space system.

14. SUBJECT TERMS
Microwave Remote Sensing, Aperture Synthesis, Soil Moisture, Ocean Salinity

15. NUMBER OF PAGES
40

16. PRICE CODE

17. SECURITY CLASSIFICATION OF REPORT	18. SECURITY CLASSIFICATION OF THIS PAGE	19. SECURITY CLASSIFICATION OF ABSTRACT	20. LIMITATION OF ABSTRACT
Unclassified	Unclassified	Unclassified	Unlimited